UNIVERSITÀ DEGLI STUDI DI PARMA

Complex emergent dynamics in neural networks with synaptic plasticity

Università degli Studi di Parma

Dottorato di Ricerca in Fisica – XXIX Ciclo

Candidate

Fabrizio Pittorino

Coordinator

Prof. Cristiano Viappiani

Thesis Advisor

Prof. Raffaella Burioni

Co-Advisors

Dr. Alessandro Vezzani

Dr. Miguel Ibáñez Berganza

A thesis submitted in partial fulfillment of the requirements
for the degree of Doctor of Philosophy in Physics

March 2017

Thesis not yet defended

Complex emergent dynamics in neural networks with synaptic plasticity
Ph.D. thesis. University of Parma

Version: February 10, 2017

Author's email: fabrizio.pittorino@gmail.com

I'll make my money square.
Scrooge McDuck

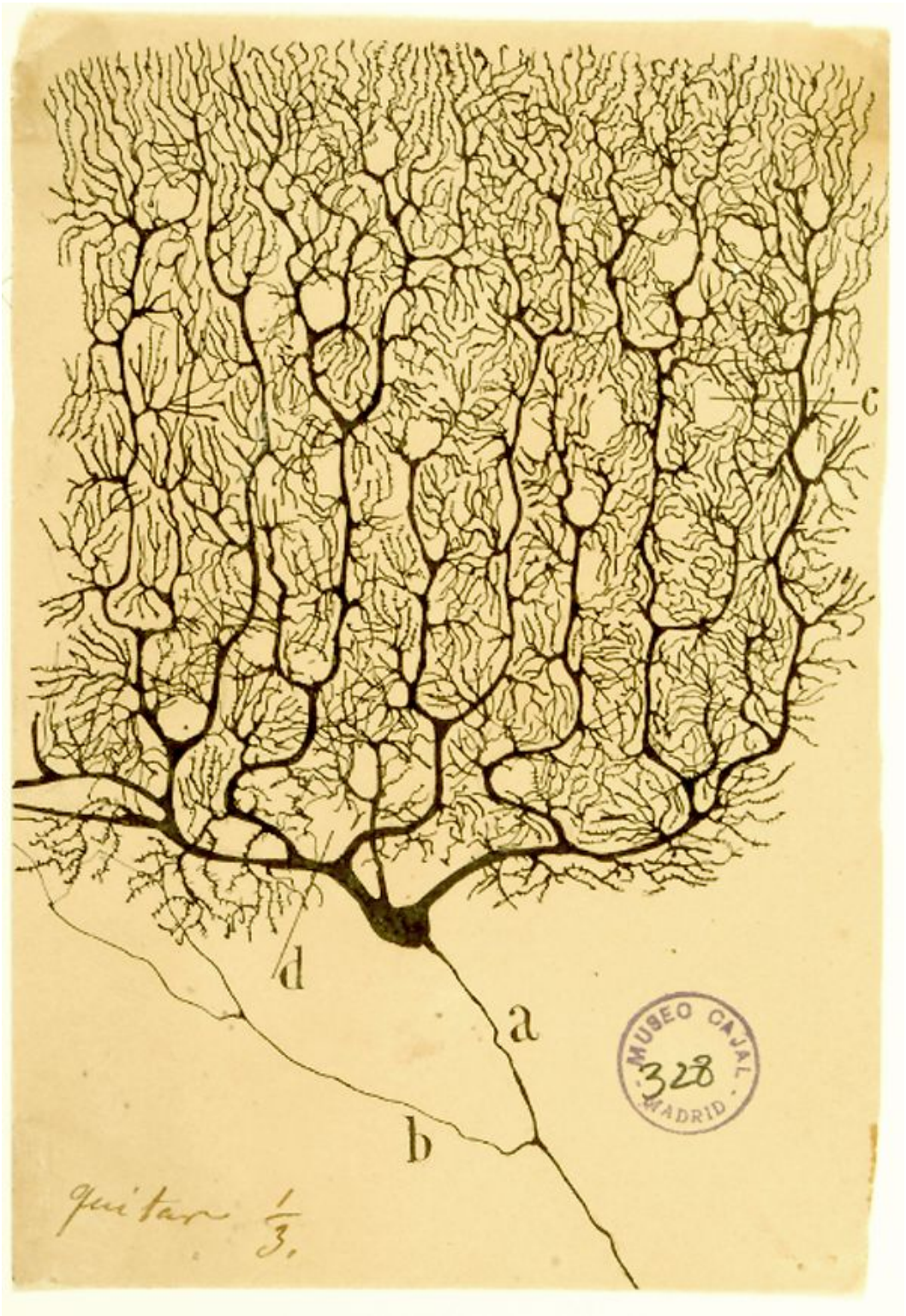

Drawing of a Purkinje cell in the cerebellar cortex done by Santiago Ramón y Cajal with Golgi's staining method - Legado Cajal, Instituto Cajal (CSIC), Madrid.

Abstract

This thesis concerns the study of the emerging dynamical regimes in a neural network in the presence of the mechanism of short-term synaptic plasticity, in the perspective of statistical mechanics. In particular, in this thesis we develop methods to characterize and to study the collective regimes present in neural systems, namely synchronization, chaos and criticality. Thanks to the measures developed in the thesis, it has been possible to draw with great precision the phase diagram (hitherto unknown) of one of the most basic and fundamental models in theoretical neuroscience, namely the leaky integrate-and-fire single neuron model connected with a Tsodyks-Uziel-Markram model for short-term synaptic plasticity. This phase diagram has been calculated with great precision in the cases of a mean field and a disordered topology. Thanks to an analytical reduction of the dynamics to a few simple coupled equations, it has been possible to elucidate the mechanism by which the model becomes chaotic in the mean field phase, preserves chaos and generates power-law distributed avalanches in the disordered topology.

Contents

Introduction

Hippocrates was among the first to understand the role of the brain in the V century BC, having intuition that this organ is the substrate for consciousness, memories, learning and, in case of perturbation of the healthy state, cause of psychiatric disorders and melancholia. It is remarkable that these are active lines of research nowadays. However, experimental basics of neuroscience date back to the XVIII century and have been pioneered by Paolo Galvani, Camillo Golgi and Santiago Ramón y Cajal. They introduced methods to study and image the brain and they are therefore considered the fathers of modern, experimental and quantitative neuroscience. In particular, their work culminated in the understanding that the brain and the central nervous system have electrical properties and are made of many interconnected cells, *neurons*, participating in the transmission of electrical signals. *Glia*, cells supporting neurons but not involved in electrical transmission, were discovered thereafter. However, the precise functional and structural role of both types of cells is still under investigation.

In 1952, the Nobel prize in Physiology or Medicine has been awarded to a fundamental step further in the understanding of electrical properties of neurons: Alan Lloyd Hodgkin and Andrew Huxley formalized the functioning of a single neuron by studying the giant squid axon, *de facto* opening the door to the possibility of understanding the mechanisms and *dynamics* of electrical potential generation by single neurons, and to its mathematical modelling.

Nowadays, the research in neural sciences has become very popular, following the previous fundamental revolution in basic biological sciences, the genome. One of the ultimate goal of this broad discipline is to understand how consciousness is processed in the brain, as well as the mechanisms of memory and learning. Basic research is thought to be fundamental also for clinical applications, being Alzheimer's disease one of the most wide-spread and impactful diseases whose origin is still unknown. A more speculative direction may be considered the uncovering of the underlying biological processes of psychiatric diseases, which would turn psychiatry and psychoanalysis in a full quantitative science. As the brain is the biological substrate of consciousness, this should be possible, at least in theory.

Neural sciences have gained the interest of scientists coming from different backgrounds and is now going in many directions. Experimental technologies are becoming more and more accurate and powerful, and mathematical modelling is therefore required in order to gain a deeper understanding of the consequent data *deluge*, that is thought to grow more than linearly in forthcoming years []. In particular, neural science, being a biological discipline, is strongly connected with statistics and computer science for what concerns machine and deep learning,

with experimental physics for what concerns imaging methods and light-based investigations (such as *optogenetics*), and with mathematics and theoretical physics (especially *statistical* physics) for what concerns modelling and inferring general understanding at *single-unit* (i.e. neuron or synapse) and *network* (interconnected assemblies of neurons) level. This is an important task in order to make the discipline *quantitative* and, hence, predictive. The latter may be considered among the most important long-term goals of a broader research line, *quantitative biology*.

Every model is far from the real complexity that is inherent in the description of every physical mechanism present in neural dynamics. On the other hand, anatomical observations suggest that real neural networks are made of a very large number of interacting neurons and, when dealing with large–scale or collective neural processes, one can expect that a high level of detail is not necessary in order to describe the fundamental aspects of collective dynamics, following the tradition of statistical physics. However, this can be argued observing that a single neuron does not play a crucial role for brain processes and cannot modify them significantly in case of inefficiency. Actually, it is well known that the brain activity is robust with respect to relatively strong perturbations.

With the aim of considering a model describing the fundamental aspects of neural dynamics we consider a system of leaky integrate–and–fire (LIF) neurons, interacting via a synaptic current regulated by the short–term "plasticity" mechanism. We remark however that the term *synaptic plasticity* usually refers to the *long term* mechanism, i.e. a physical modification in the structure of neural connections. With a lexical abuse the scientific literature extends the term plasticity to the short-term mechanism, but we stress that this is a process involving only a modification in the quantity of neurotransmitters available in spike transmission from neuron to neuron and not to a modification in the biological structure of neural ramifications. As the model for the underlying topology we consider the simplest fully mean field case and randomly uncorrelated diluted networks in the thermodynamic limit, thanks to an approximation named Degree based Mean Field.

This thesis deals with Statistical Mechanics and with the possibility to adapt concepts and technologies taken from this discipline to the neural sciences. Statistical Mechanics is a well established quantitative discipline, which among the centuries has developed powerful mathematical tools with the aim to unravel the statics and the dynamics of a plethora of condensed matter models made of many elementary interacting constituents. Its application to the neural sciences appears therefore well grounded, as neural networks are composed of many interconnected units. We stress that this is the perspective from which this thesis has to be interpreted, and that this is its main aim of research.

The thesis is organized in three Chapters. In the first Chapter we describe the experimental observations of neural dynamics, and how it is possible to construct mathematical models of a neural network from physiological observations. In the second Chapter we report the main features of the dynamics of the fully mean field case of the neural model introducted in the previous Chapter. We find a form of synchronous chaos in a purely excitatory network, in the presence of the mechanism of synaptic plasticity. In the third Chapter we study how the introduction of disorder in the topology of this mean field excitatory network has an interplay with the chaotic phase and how this mechanism gives rise to a regime that has been experimentally

observed, characterized by power law distributed bursts of activity, or so called *avalanches*.

Part I

General overview: Statistical Physics and the Brain

Chapter 1

From biology to models for neural networks

The *brain*, besides being the most complex known object in our universe, is the organ coordinating the behaviours of a variety of animals going from the fruit fly to the large mammals and ultimately to its most accomplished version, the homo Sapiens. Our brain is our main peculiarity with respect to the other species in the animal kingdom. The role of this organ is to elaborate the sensory stimuli coming from the environment and to drive the response of the body. A crucial question is to understand the way the brain elaborates information and "takes decisions" to the motor and cognitive levels. Thanks to the technological advancement for what concerns experimental techniques it has been possible to deduce that the fundamental functional units composing the brain are the cellular elements, called *neurons*. They are able to emit and propagate electrical potentials to other neurons, called *spikes*.

The fundamental measurable quantity when speaking of neurons is the *electrical potential*. The electric fields emitted by the brain may be measured through e.g. electroencephalography (EEG) and are used to quantitatively describe macroscopic (and therefore mediated) brain activity. Several other methods to study brain function exist, e.g. magnetic resonance imaging (MRI) (Figure 1.1), positron emission tomography (PET) and magnetoencephalography (MEG).

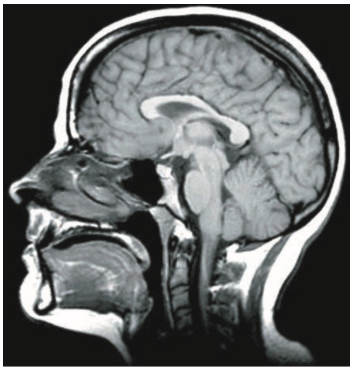

Figure 1.1. The major anatomical divisions are evident in a magnetic resonance image of a living human brain [37].

Microscopic measurements are accurately executed through an experimental techniques called *patch clamp* (it is possible to record single neuron electrical activity as well as how interactions occur between neurons). Notably, the microscopic measurements (corroborated by macroscopic ones) are precise enough to construct mathematical models for single and collective neural activity, which can be compared back with experimental measurements, and that, hopefully, are predictive.

In this chapter we discuss how it is possible to infer, from experimental evidence, mathematical models of single neuron and synapses and how the latter two elements may be connected in a *network*.

1.1 The individual Brain cells: Neurons

1.1.1 Experimental basics and Neuron physiology

Over the past centuries, structure and function of the brain have been explored in great detail. It has been realized that the elementary processing units in the brain are cells named neurons, interconnected to each other in a *network*.

The brain is composed by 10^{11} neurons connected to each other. Anatomical evidence indicates that neurons in human brain have on average $10^3 - 10^4$ connections to their neighbours and that in the cerebral cortex the density of neurons reaches 10^4 cell bodies per mm^3. The topology of the brain network results different across different areas of the brain itself. There are various types of neurons, and also a large number of glia cells, that are required in order to support neurons with energy and structural stability of the network. But glia cells are not involved in information processing and consequently their behaviour appears to be less complex than the one of neurons.

The peculiar characteristic of neurons is their electrical activity, measured in terms of their membrane potential V, which indicates the difference between the voltage outside and inside the cellular body. In absence of perturbations the membrane potential stays at a resting potential V_r. When V, because of external stimuli, exceeds a certain threshold value it undergoes a rapid rising followed by a rapid coming back to the resting value of the potential: this phenomenon is called generation of an *action potential* and has a stereotyped shape.

This electric signal travels along a nerve fiber called *axon* and is carried to other neurons by means of branches called *dendrites*, while the points of connection between the axon and the target cells are referred to as *synapses*. At the synapse the sequence of action potentials of the pre-synaptic neuron influences the potential of the post-synaptic neuron, increasing or decreasing it.

The dendrites collect signals from other neurons and transmit them to the soma. This cellular body may be considered a processing unit that evolves non linearly the total input arriving to it. If the latter exceeds a certain threshold, then an output signal is generated. The axon then has the role of delivering the signal to other neurons.

All neurons share the same qualitative anatomical structure of the soma, and different neurons can have different dendritic ramifications. Following the above discussion, a neuron may be divided into three main functionally distinct parts, called dendrites, soma and axon, as shown in Figure 1.2.

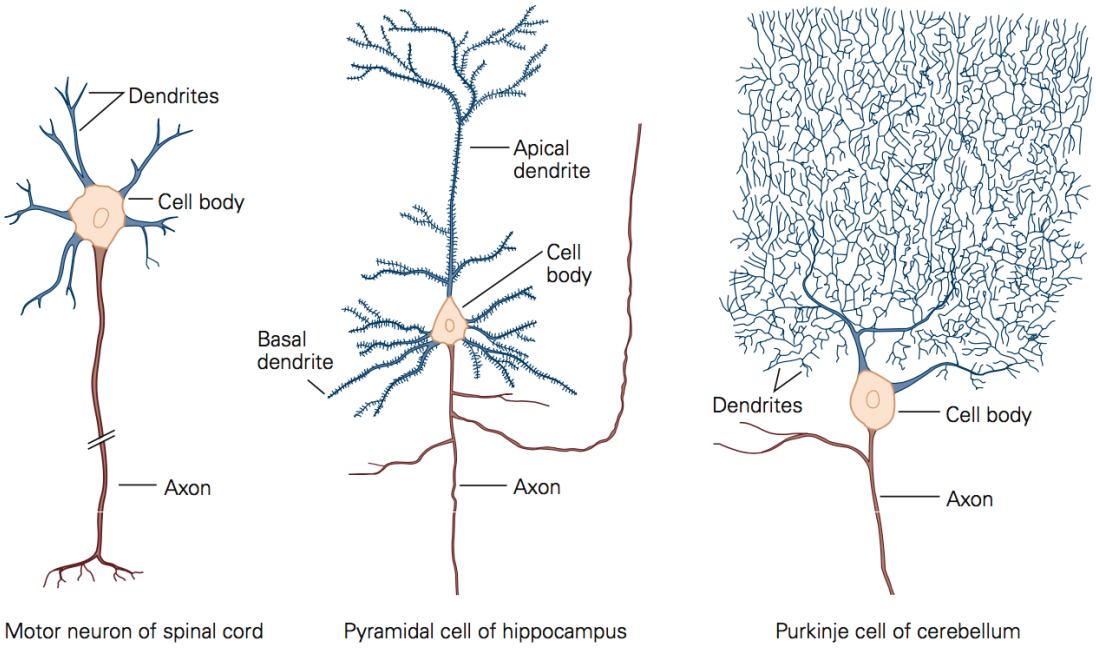

Figure 1.2. Multipolar cells have a single axon and many dendrites. They are the most common type of neuron in the mammalian nervous system. Three examples illustrate the large diversity of the possible cellular bodies and ramifications [37].

Chemical mechanisms are at the basis of the electrical activity of neurons, which makes neural tissues able to generate electric fields that can be measured at the global level by electroencephalography (EEG), a technique successfully used for the first time in 1924 by Hans Berger [29]. EEG is not invasive, as it reveals the electric field positioning electrodes on the head, but it is limited in spatial resolution. It is currently used in medical diagnostic as it is useful to recognize, as an immediate application, coma or brain death. A notable example is that an important neurological disease, epilepsy, is characterized by an excess of synchronization.

The intensity of the electric fields generated by a single neuron cannot be detected by EEG. The resulting signals are therefore the result of the constructive interference of single neurons activity and reflect the synchronization properties of the neurons in the cerebral area investigated by the different electrodes. The synchronization of neurons gives rise to oscillations in certain frequency bands in their mean activity, that can be revealed and measured by EEG: alpha ($8-13$ Hz), delta ($0.5-4$ Hz), theta ($4-8$ Hz), beta ($13-30$ Hz) and gamma ($30-70$ Hz). In Figure 1.3 we report some examples of measured collective oscillations associated with the brain state to which they correspond.

Frequency Band Name	Frequency Bandwidth	State Associated with Bandwidth	Example of Filtered Bandwidth
Raw EEG	0–45 Hz	Awake	
Delta	0.5–3.5 Hz	Deep Sleep	
Theta	4–7.5 Hz	Drowsy	
Alpha	8–12 Hz	Relaxed	
Beta	13–35 Hz	Engaged	

Figure 1.3. Some examples of EEG recordings [47].

An important step forward to move the experimental analysis to a microscopic level has been the possibility to create cultures of interconnected neurons in laboratories. Through the use of micro electrodes measurements (a pattern of electrodes used to detect spiking events) it is possible to have access to the dynamics of single neurons. The neuronal signals consist of short electrical pulses and can be observed by placing a fine electrode either on the soma or close to the soma or axon of a neuron, see Figure 1.4.

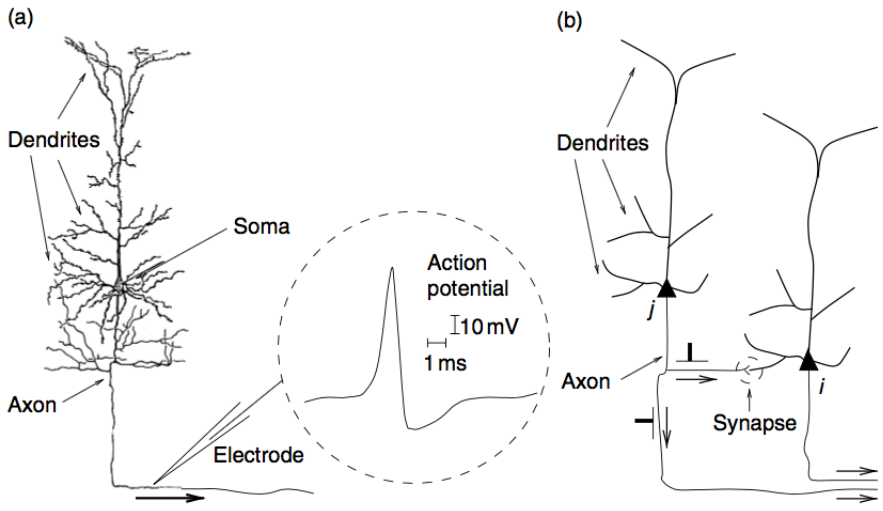

Figure 1.4. (a) Single neuron in a drawing by Ramón y Cajál. Dendrites, soma, and axon can be clearly distinguished. The inset shows an example of a neuronal action potential. (b) Signal transmission from a presynaptic neuron j to a postsynaptic neuron i. [27].

The microscopic experimental measurements basically culminate in the *raster plot*, reporting the neuron index on the ordinates and the time on abscissa. The raster plot, at variance with the EEG recordings, is a microscopic picture of the system dynamics representating the timing at which every neuron emits a spike: each time an event (a spike) occurs, a dot is drawn at the relative time and neural index. The interpretation of this temporal series on a biological and quantitative ground poses a formidable challenge. An example of raster plot is reported in Figure 1.5.

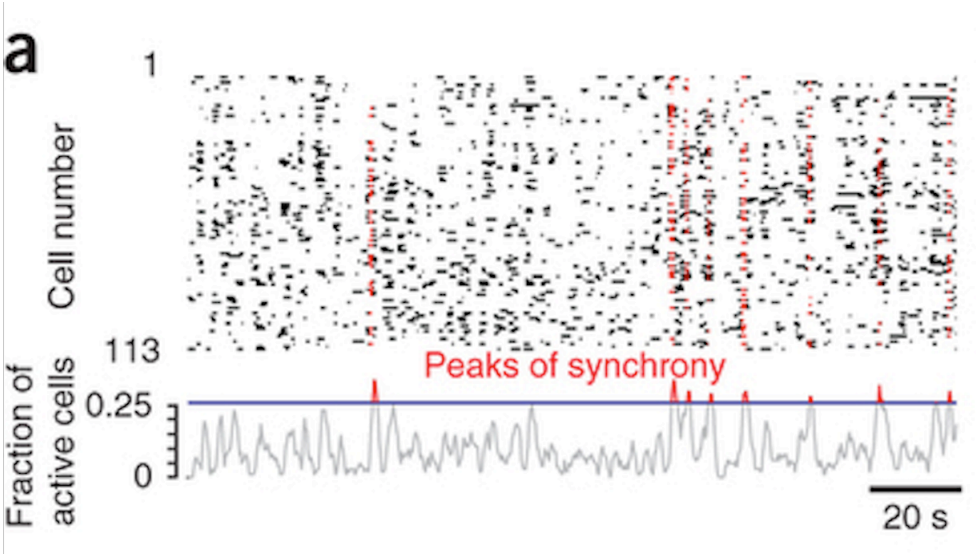

Figure 1.5. Raster plot and activity density [28].

An important representation of the dynamics of neural systems that will be explored in this thesis and that is represented in Figure 1.5 are *bursting events*, usually called population bursts (PB), where a large fraction of neurons fire in a short interval (typically of hundreds of ms). When a PB appears, the collective activity shows a peak, and this can happen at irregular times, giving rise to a phenomenon of synchronization without periodicity. The distribution of times between two consecutive PB, such as the one representing the distribution of the fraction of neurons emitting a spike in each PB (also called the distribution of *avalanches*) follows a long tail statistics with rare events, usually a power-law.

The synchronization between neurons appears therefore to be a fundamental aspect for what concerns the collective dynamics of neural systems, both in cultures (*in vitro*) and at the global level as recorded through EEG *in vivo*. Different mathematical models may give rise to synchronization in systems of non-linear dynamical units connected by eventually dynamical and non-linear couplings.

1.1.2 Neuron dynamics

The state of the neuron is described by its membrane potential V, defined as the potential difference between the cell body and the extracellular liquid around the neurons themselves. In absence of external perturbations the cell membrane has

already a strongly negative polarization of about $V_r = -65$ mV, where V_r represent therefore the constant membrane potential corresponding to the resting neuron.

The effect of a spike on the postsynaptic neuron can be recorded with an intracellular electrode which measures the potential difference V. Whenever V exceeds a certain threshold value, due to an external perturbation, a rapid increase of V occurs, called *polarization*, followed by a rapid decrease to a value lower than V_r. A third phase called iperpolarization brings V again to the resting value V_r and the neuron has the possibility to emit another spike. This rapid rise and fall of V in time is called *action potential*.

If the change in the membrane potential consequently to a spike is positive, the synapse is said to be excitatory. If the change is negative, the synapse is inhibitory. An input at an excitatory synapse reduces the negative polarization of the membrane and is therefore called depolarizing. An input that increases the negative polarization of the membrane even further is called hyperpolarizing. In this thesis we will deal with excitatory synapses only.

The action potentials have an amplitude of about 100 mV and typically a duration of $1-2$ ms, and they propagate along the axon. Action potentials (also called *spikes*) have a stereotyped shape depicted in Figure 1.6. This is a strong indication that the form of the action potential does not carry information.

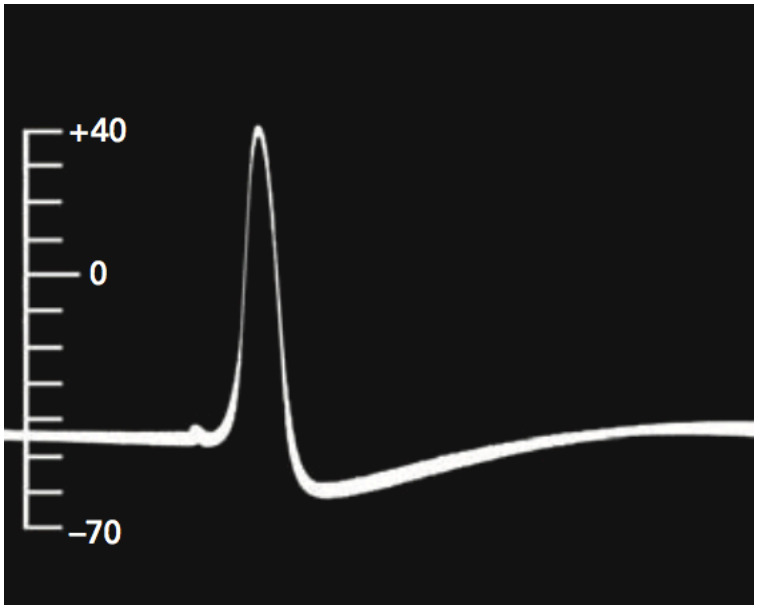

Figure 1.6. The first published intracellular recording of an action potential. It was recorded in 1939 by Hodgkin and Huxley from a squid giant axon, using glass capillary electrodes filled with sea water. The timing pulses are separated by 2 ms. The vertical scale indicates the potential of the internal electrode in millivolts, the sea water outside being taken as zero potential.

A chain of action potentials emitted by a single neuron is called a spike train. This temporal series may be regarded as a robust description of the neural code: it is the number and the timing of spikes which carry all the relevant information, the *language* through which neurons communicate. The action potential is then the

elementary unit of signal transmission and they usually result well separated in a spike train. Even with very strong input, it is impossible to excite a second spike during or immediately after a first one: this is called *refractory period*. The absolute refractory period is followed by a phase of relative refractoriness where it is difficult, but not impossible, to excite an action potential.

The general mechanisms underlying the generation of the action potential has been unraveled by a pioneering experiment on the squid giant axon, leading to the Nobel prize in Physiology or Medicine in 1952 to Hodgkin and Huxley. Their precise measurements, together with an elegant and (apparently) simple mathematical description of neuron dynamics opened new possibilities in the quantitative understanding of spike generation and emission [34]. They realized that the mechanism through wich neurons are capable of changing their polarization is the capability of regulation of ionic currents passing through the membrane of neurons themselves. The principal currents are associated with sodium (Na^+), potassium (K^+), calcium (Ca^{2+}) and chlor (Cl^-) ions. Neurons are capable of pumping ions of different signs inside and outside the cell and to generate in this way electrical activity. The mathematical model for the dynamics of V developed by Hodgkin and Huxley takes into account Cl^- and K^+ currents, explanaining the mechanism of formation of the action potential. The Hodgkin Huxley (HH) model is made of four coupled differential equations, making it too complex for computational experiments, not mentioning analitical investigation. This led to a (successful) search for simpler current-based models, like the Morris Lecar and the FitzHugh Nagumo one, obtained by a dimensional reduction of the HH set of equations.

1.1.3 The simplest membrane potential equation: integrate-and-fire models

To a first approximation, neuronal dynamics can be conceived as a summation process (*integration* process of the incoming inputs to a certain neuron) combined with a mechanism that triggers action potentials above some critical voltage. In experiments firing times are often defined as the moment when the membrane potential reaches this threshold value from below. If the shape of an action potential is always the same, then the shape cannot be used to transmit information: rather information is contained in the presence or absence of a spike. Therefore action potentials may be considered *events* that happen at a precise moment in time.

Neuron models where action potentials are described as events are called *integrate-and-fire* models. This class of models makes use of the fact that neuronal action potentials of a given neuron always have roughly the same form, and no attempt is made to describe the shape of an action potential.

Integrate-and-fire models have two separate components that are both necessary to define their dynamics: first, an equation that describes the evolution of the membrane potential V; and second, a mechanism to generate spikes.

The simplest model in the class of integrate-and-fire, capturing some of the most fundamental elements of neuron dynamics is the *leaky integrate-and-fire* (LIF[1]), already introduced in its simpler form by Lapicque in 1907 [40]. This model is

[1]Generalized integrate-and-fire models can be seen as variations of this basic model.

not current-based and is an extreme semplification taking care of only the most fundamental aspects of single neuron dynamics, i.e. the presence of a threshold value (V_{th}) and a resetting mechanism to the value V_r (the resting potential).

The equation of the LIF model is therefore:

$$\tau_m \dot{V} = E_l + V_r - V \tag{1.1}$$

$$\text{if } V > V_{th} \rightarrow \text{delta-shaped spike emission and reset: } V = V_r, \tag{1.2}$$

τ_m is a time constant that takes into account the capacity of the cell membrane. This equation can be considered the one of a capacitor in the presence of a leakage term, E_l. This term represents the leakage current that flows through the membrane because of different concentrations of ions inside and outside the soma (this mechanism is fundamental for making V come back to its resting value V_r in absence of stimuli).

In the LIF equation, this mechanism is approximated by resetting by hand the potential V when it exceeds a certain threshold V_{th} to the value of the resting potential V_r. Furthermore, the action potential is considered instantaneous and the spike train can be modeled as a series of Dirac delta functions.

It is possible to rescale time and voltages in order to introduce adimensional variables and to simplify the mathematical and computational treatment of the equations [2]. We can therefore introduce the rescaled quantities:

$$t \rightarrow \frac{t}{\tau_m} \tag{1.3}$$

$$v = \frac{V - V_r}{V_{th} - V_r} \tag{1.4}$$

The equation for the dynamics of v becomes:

$$\dot{v} = a - v, \tag{1.5}$$

where a is the rescaled leakage current, the resting value becomes $v = 0$ and the threshold value $V_{th} = 1$.

Physiological values for these parameters are $\tau_m = 30$ ms, $V_r = -65$ mV and $V_{th} = 55$ mV. In the rescaled equation, a becomes the only parameter of the single neuron dynamics.

It is possible to analize the dynamical properties of the LIF model for $v(t)$. If $a > 1$, v follows a periodic dynamics of period:

$$T = \ln\left(\frac{a}{a-1}\right) \tag{1.6}$$

and spikes are emitted at regular rate. The time lapse between two consecutive spikes, called inter–spike–interval (ISI), is constant and equal to T, making this regime periodic. On the contrary, if $a < 1$ the dynamics of v has a stable fixed point $v = a$ and the neuron does not emit spikes. In Fig. 1.7 we show the spiking dynamical regimes.

[2] To read the results in physical units, voltage and time have in this way to be rescaled consequently.

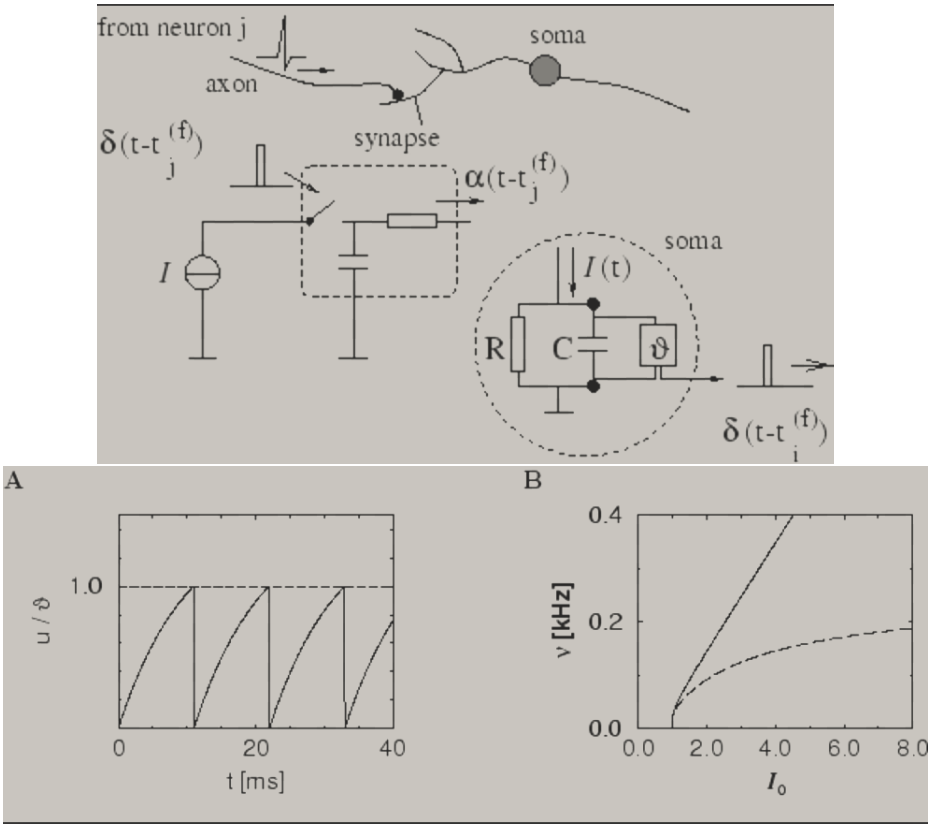

Figure 1.7. Upper panel: schematic representation of the LIF model as an RC circuit. Lower panel left: rescaled membrane voltage potential in function of time. Lower right panel: response curve of the frequency of the LIF model in function of an external input current, showing its belonging to class I excitability.

The LIF model has the advantage to be computationally efficient and analytically integrable between two consecutive spikes. However, it has to be pointed out that it is not able to describe specific characteristics of neural dynamics as the formation of action potentials. The leaky integrate-and-fire model is an extremely simplified neuron model: it neglects many features that have been observed in neurons in the living brain or in slices of brain tissue. We cannot expect the LIF to explain the complete biochemistry and biophysics of neurons. Nor do we expect it to account for highly nonlinear interactions that are caused by active currents on the dendritic tree.

A model of spike generation should be able to predict the moments in time at which a real neuron spikes. The LIF model is surprisingly accurate when it comes to generating spikes, i.e., precise events in time. Thus, it could potentially be a valid model of spike generation in neurons, or more precisely, in the soma.

The main methods shown in this thesis can be applied also to more complex neural models (and this is an immediate extension and prospective of this work). Nevertheless, we will deal with LIF neurons that permit an easier analytical and computational treatment and an easier interpretation.

In the next sections it will be shown how one can write down a model for dynamical units connected together that will be used in the rest of the thesis to

investigate the complex dynamics of neural networks.

1.2 Interconnected Neurons

As we have seen in the precedent section, the central part of cells in general and of the neuron in particular is the soma, which contains the nucleus with the genetic information and the molecular machinery of the cell. From the soma of the neuron originate two types of extensions. The first type is represented by the dendrites, a multitude of branches of different size on which the junctions between two neurons are located. Second, also originating at the soma, is the axon, which the neuron uses to send action potentials to its target neurons. The site where the axon of a neuron makes contact with the dendrite (or soma) of another neuron is called *synapse*. The neuron sending a spike is referred to as the presynaptic cell and the receiving the information neuron as the postsynaptic one. Synapses are contact points through which the electrical signal and thus the information content from presynaptic neurons is transmitted to the postsynaptic ones.

It has to be stressed that conductance-based models, such as the Hodgkin–Huxley one, as well as LIF models disregard the spatial structure of neurons and reduce them to point-like spike generators – despite the fact that the precise spatial layout of a neuron could potentially be important for signal processing in the brain.

1.2.1 Synaptic connections

We focus now on the properties of the synaptic contact points between neurons. There are two types of synapses: electrical [3] and chemical, which are most common in the vertebrate brain. At a chemical synapse, the axon terminal does not come in contact with the dendrites of the postsynaptic neuron, leaving only a small region between the membranes of the presynaptic and postsynaptic neurons, called the *synaptic cleft*.

When the cell body of the presynaptic neuron produces an action potential, it propagates pretty fast as a wave along the axon (around $25\,\mathrm{ms}^{-1}$). When the action potential arrives at a synapse, it triggers a complex chain of biochemical processing steps that lead to a release of neurotransmitter from the presynaptic terminal into the synaptic cleft. When it arrives at the axon terminal it induces the opening of Calcium channels. The ratio between Ca^{2+} concentration inside and outside the cell is around 10^4 and this provokes a gradient of ions flowing inside the axon terminal. In the axon terminal there are vescicles that, whenever a presynaptic neuron is activated and calcium concentration increases around it, release molecules said neurotransmitter (or resources) into the synaptic cleft. The transmitter molecules diffuse to the other side of the cleft and activate ion channels

[3] In electrical synapses (sometimes called gap junctions) the axon and the dendrites come in contact and the electrical signal passes directly from a neuron to the other. Specialized membrane proteins make a direct electrical connection between the two neurons. Not much is known about the functional aspects of gap junctions, but they are thought to be involved in the synchronization of neurons. However, electrical synapses are rare in the nervous system which is mostly connected through chemical synapses.

(activated by transmitter from outside the cell) that are located in the post-synaptic membrane.

As soon as transmitter molecules have reached the postsynaptic side, they bind to specific receptors in the membrane of the postsynaptic side of the synapse and generate the opening of specific ionic channels causing ions from the extracellular fluid to flow into the cell. In Figure 1.8 we show a schematic description of this picture.

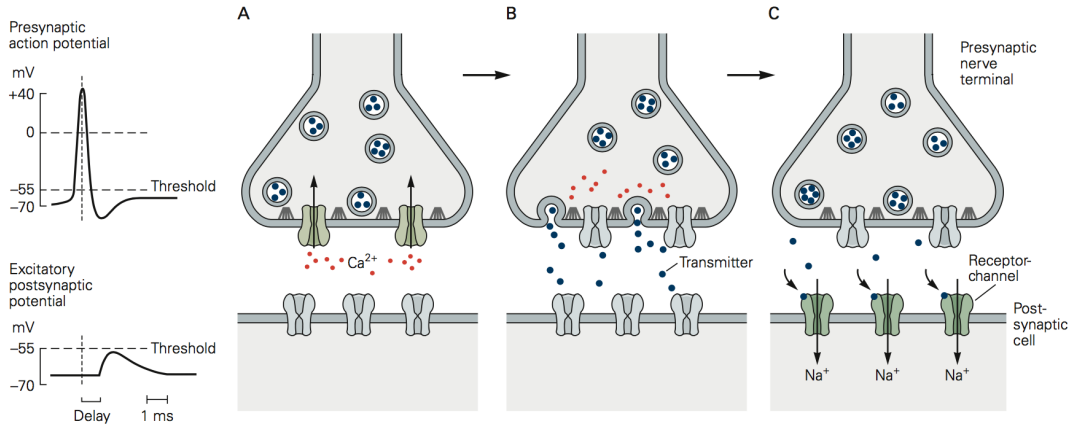

Figure 1.8. Synaptic transmission at chemical synapses involves several steps. The complex process of chemical synaptic transmission accounts for the delay between an action potential in the presynaptic cell and the synaptic potential in the postsynaptic cell, compared with the virtually instantaneous transmission of signals at electrical synapses. [37].

The ion influx, in turn, changes the membrane potential at the post-synaptic site. This mechanism determines the postsynaptic current I_{syn} that rules the change in the postsynaptic neural membrane potential. In the end, the chemical signal has been translated into in an excitatory or inhibitory postsynaptic transmembrane current and therefore an electrical response. The voltage response of the postsynaptic neuron to a presynaptic spike is called the postsynaptic potential.

Excitatory and inhibitory synapses

There are different chemical type of neurotransmitter: one of the most famous is the amino acid GABA [26]. When this neurotransmitter is released, the current I_{syn} flowing in postsynaptic neuron is negative reducing postsynaptic neuron excitability. This type of neurotransmitters are said inhibitory. On the contrary, glutamate is a neurotransmitter said excitatory as it generates a positive current I_{syn} in postsynaptic terminal. A neuron whose neurotransmitters are excitatory or inhibitory is said as well excitatory or inhibitory, respectively. In the rest of this thesis we will concentrate on excitatory neurons, where we use the term excitatory related to the neuron and not to the synapse, even if in some cases the same neuron produce either inhibitory or excitatory post-synaptic signal in the target cell. In general the percentage of inhibitory neurons is lower than that of excitatory neurons, around $10 - 30\,\%$ [2].

1.2.2 The synaptic plasticity Tsodyks-Uziel-Markram equations

Once investigated the dynamics of the single neuron and built up a model for the dynamics of the membrane potential in absence of stimuli from other neurons, it is necessary to take under consideration the coupling dynamics. From an experimental point of view this means to quantify the effect of the spike train of a neuron into the membrane potential of the receiving one.

As the action potential has a stereotyped shape, the neurotransmitter properties are responsible of the intensity of postsynaptic currents. These properties are able to modify in time and change the efficiency of a synapse. Furthermore, the creation of new synapses is possible, resulting in a change of the network structure. These mechanisms are called *synaptic plasticity* and they are generally thought to be responsible for memory and learning.

There are two main forms of synaptic plasticity: long and short term plasticity. They differ mainly for the time scales ruling the process. Furthermore, in the short term plasticity mechanism, the synaptic efficiency depends only on the dynamics of presynaptic neuron, i.e. from its spike train, and does not affect the structure of connections, at variance with long term forms of plasticity.

In this thesis we will take into account the short term plasticity mechanism, for which a mathematical model that reproduces the experimental observations has been constructed. From the observation of the electrical activity of pairs of neocortical pyramidal neurons of the rat, in [65] it is reported a model for short–term–plasticity between excitatory neurons. It is based on the dynamics of synaptic resources (i.e. neurotransmitters), which depends basically on the presynaptic spike train. The resources may assume three different states: there is a fraction of available resources x, a fraction of active resources y and a fraction of inactive resources z.

Their dynamics are described by the following dynamical equations for the presynaptic neuron i:

$$\dot{y}_i = -\frac{y_i}{\tau_{in}} + U x_i S_i \tag{1.7}$$

$$\dot{x}_i = \frac{z_i}{\tau_r} - U x_i S_i \tag{1.8}$$

$$\dot{z}_i = \frac{y_i}{\tau_{in}} - \frac{z_i}{\tau_r} \tag{1.9}$$

where

$$S_i(t) = \sum_n \delta\left(t - t_{n,i}\right) \tag{1.10}$$

is the spike train, U is a parameter, and τ_{in} and τ_r are said inactivation and recovery time, respectively. With this definition of spike train, each action potential is described by a Dirac delta function that is non-zero at the times when the n–th action potential is emitted by neuron i. Notice that, by construction, the sum of all the fraction of resources is equal to one, i.e.:

$$x_i + y_i + z_i = 1. \tag{1.11}$$

Whenever a spike is emitted by neuron i a fraction U of the available resources x_i passes immediately from the available to the active state, i.e.:

$$\Delta y_i = U x_i \tag{1.12}$$
$$\Delta x_i = -U x_i. \tag{1.13}$$

In between two consecutive spikes, the active resources y_i responsible for the postsynaptic current $I_{syn,\,j}$ flowing in neuron j become inactive exponentially with a time scale τ_{in}. Consequently, the inactive resources z_i of neuron i grow of the same amount.In the meanwhile, the fraction of available resources x_i recovers exponentially from the fraction of inactive resources z_i with a time scale τ_r.

The postsynaptic current is proportional to the fraction of active resources y_i, i.e.

$$I_{syn,\,j} = c\, y_i. \tag{1.14}$$

The mechanism described by Equations (1.8) is named *depressive*, indicating that if the presynaptic neuron fires with high frequency, the synapse efficiency becomes negligible as there are no more available resources.

1.3 Biological Neural Networks

Neurons are embedded in a network of billions of other neurons and glial cells that make up the brain tissue. The brain is organized into different regions and areas. The cortex can be thought of as a thin but extended sheet of neurons, folded over other brain structures. Some cortical areas are mainly involved in processing sensory input, other areas are involved in working memory or motor control. Neurons in sensory cortices can be experimentally characterized by the stimuli to which they exhibit a strong response.

In previous section we have discussed the observed features of neurons and synaptic dynamics derived from experiments. We are now able to develop a model that reproduces quantitatively the firing patterns of ensembles of neurons observed in experiments, and hopefully the complex dynamics arising from their interactions. To do so, we have to develop a model for a *neural network*, making use of graph and network theory.

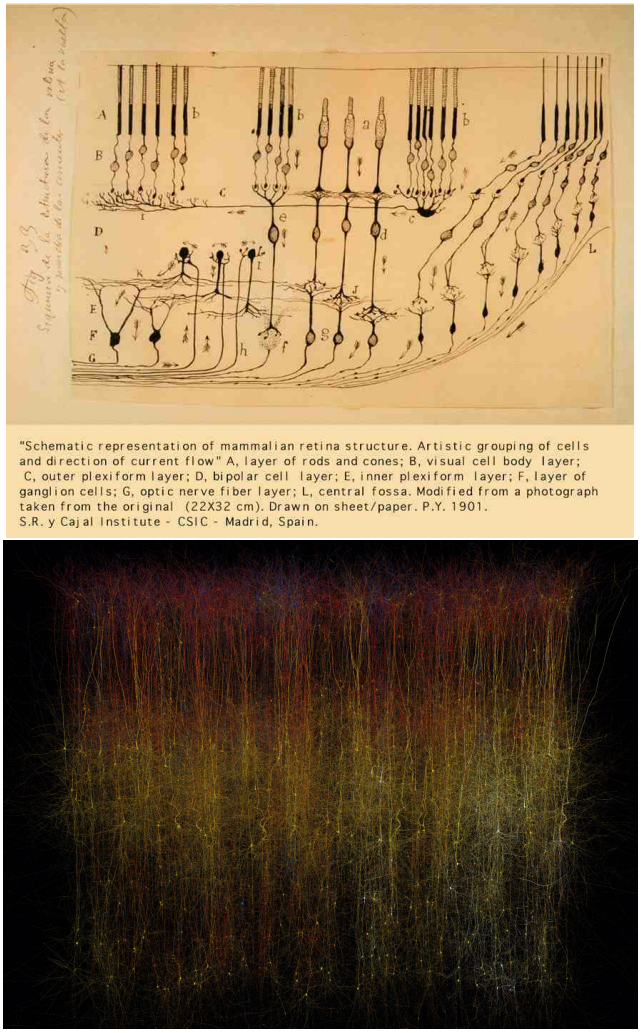

Figure 1.9. Top: Neural network as first drawn by Santiago Ramón y Cajal. Bottom: computer reconstruction of a neural column in the cerebral cortex by the Blue Brain Project.

1.3.1 Graph and network theories in a nutshell

In order to study the dynamics of extended systems, like neural ensembles, one has to define the structure of connections between single units. Graph theory is the mathematical framework to characterize the network of connections.

A graph can be defined as set V of nodes together with a set E of edges. Nodes represent the dynamical units of the system while edges the connections between single nodes.

Graphs can be divided in two main families, undirected and directed graphs. The first class is characterized by edges with no preferential direction. This means that, if a connection exists between node i and j, the influence of one on each other is bidirectional. This case applies in epidemic spreading models [6] where there is no directionality in the coupling between two nodes that infect each other when they come in contact.

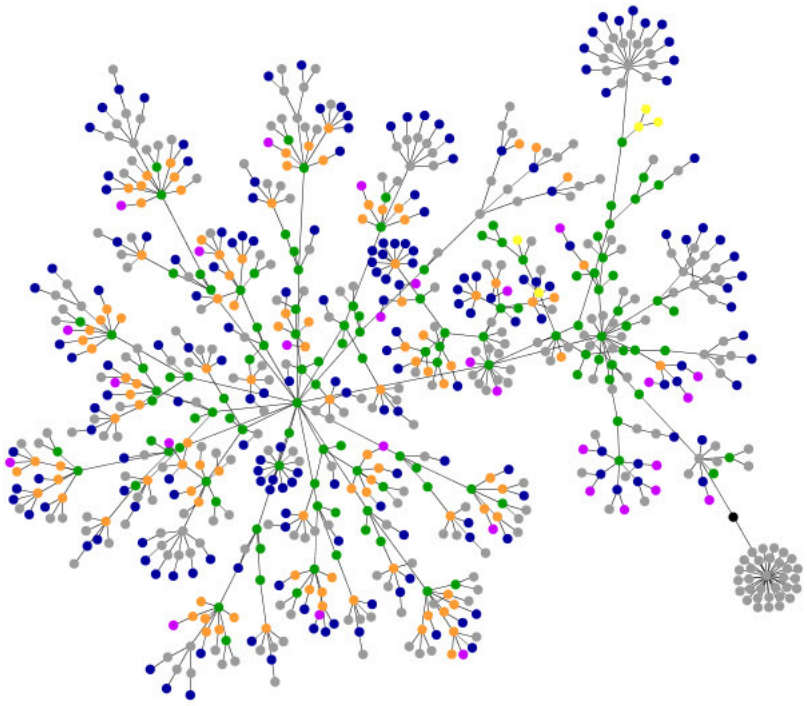

Figure 1.10. Example of an undirected network.

On the contrary, in neural systems the coupling is directional as the axon of neuron i can come in contact to a dendrite of neuron j and not vice versa. Thus, neuron i can send spikes to neuron j but not necessarily neuron j affects neuron i dynamics. This class of graphs are called directed and the edges are usually called arcs or arrows.

A graph formed by N nodes can be represented by a $N \times N$ matrix ϵ_{ij}, called adjacency matrix. Its entries ij are 0 or 1. If node j is directly connected to neuron i: $\epsilon_{ij} = 1$, otherwise $\epsilon_{ij} = 0$. By definition, if the graph is undirected the adjacency matrix is symmetric.

A first quantity that plays a fundamental role in the dynamics of the units is their connectivity. In the case of directed graph there are two different possible definitions. The in–degree and the out–degree connectivity are respectively

$$k^i_{in} = \sum_j \epsilon_{ij} \tag{1.15}$$

$$k^i_{out} = \sum_j \epsilon_{ji}. \tag{1.16}$$

Given a certain graph of size N we can define $P(k_{in})$ the in-degree or connectivity distribution of the network. In finite size samples this distribution is the envelop of the histograms obtained analyzing the connectivity of the nodes. As $k_{in} \in [0,\, N-1]$ in order to avoid self loops, P needs to be suitably normalized.

There are several ways to construct networks. In this thesis we will consider random and uncorrelated network. A random network is a network constructed with some random process that can be defined by a probability distribution or by the

random process which generates it. Uncorrelated graphs are graph for which the probability that a neuron with connectivity k_{in} is connected with a neuron with connectivity k'_{in} does not depend on k'_{in}.

The most used model to generate random uncorrelated graphs is the Erdös-Rényi model. It consists in choosing every couple of nodes (i, j) and connecting them with a certain probability p. The resulting connectivity distribution $P(k_{in})$ turns out to be binomial

$$P(k_{in}) = \binom{N-1}{k} p^{k_{in}} (1-p)^{N-1-k_{in}} \tag{1.17}$$

If the size N is sufficiently large and p is fixed the central limit theorem implies that $P(k_{in})$ is a Gaussian distribution with average and variance respectively

$$\langle k_{in} \rangle = pN \tag{1.18}$$
$$\sigma^2_{k_{in}} = Np\,(1-p)\,. \tag{1.19}$$

Many networks, including World Wide Web links and social networks, show a different distribution for $P(k_{in})$ with respect to the Erdös-Rényi model, namely power law. The mostly used generative model for scale-free networks is Barabási and Albert's generative model in which each new node creates links to existing nodes with a probability distribution proportional to the nodes in-degree at each step of the generation process.

A clever way to construct random graphs with desired distribution $P(k_{in})$ is the configuration model [16]. Chosen a normalized distribution $P(k_{in})$, a sequence of N values of k_{in}

$$(k^1_{in},\, k^2_{in},\, \ldots,\, k^N_{in}) \tag{1.20}$$

are extracted by $P(k_{in})$. Then, randomly chosen k_{in} nodes indexes are assigned to each node i.

Two important classes of networks construction are sparse and dense (or massive) networks. In sparse networks the rescaled connectivity of the nodes k_{in}/N goes to zero in thermodynamic limit, while in massive networks the connectivities scale at least as the number N of nodes. In the case of Erdös-Rényi model this distinction is ruled by the dependence of p by N. If p/N does not go to zero in the thermodynamic limit the network is said massive and sparse otherwise.

1.3.2 Dynamical units interacting on arbitrary network topology

As we have seen in previous Sections, the cell body of a neuron may be modelled as a dynamical unit. The latter may be described by a vector of generic time dependent variables, $\mathbf{w}(t)$. In absence of external stimuli - or connection with other units - $\mathbf{w}(t)$ has its own dynamics, that can be written as

$$\dot{\mathbf{w}} = \mathbf{F}(\mathbf{w}) \tag{1.21}$$

where the vectorial function $\mathbf{F}$ represents the parameter-dependent single unit dynamics. Furthermore, each unit i receives a certain number of inputs that

produces a change in the dynamical variable $\mathbf{w}_i$ of the cell body. In many models of oscillators, in particular in neural systems, the effect of node j on node i depends on the state of node j, in the context of a neural network by its the spike train. Therefore, we consider this class of models by defining a general function $G(w_j)$ defining the effect of unit j on unit i:

$$\mathbf{w}_i = \mathbf{F}(\mathbf{w}_i) + g\mathbf{G}(\mathbf{w}_j), \tag{1.22}$$

where g is the coupling constant. In general, we should consider a parameter dependence of $\mathbf{G}$ in function of the unit j, but we will restrict ourselves for the sake of simplicity and tractability to a fixed setup for each neuron.

In the following we will adapt the model to identical excitatory neurons interacting on an arbitrary topology. In order to describe the collective and emergent dynamics of a neural network, we will formulate the basic model that can serve as the backbone of more sophisticated and complicated treatments: an ensemble of a certain number N of dynamical units connected on a graph. We expect, as usual in statistical mechanics, that a oversimplified model will be able to pinpoint the most important ingredients and features of the dynamics and of the stationarity properties.

To obtain the dynamics of node i on a graph we need to add the effect of all nodes sending outputs to i. If the structure of the network is described by the adjacency matrix ϵ_{ij} we can write, for each node $i \in [1, \ldots, N]$:

$$\mathbf{w}_i = \mathbf{F}(\mathbf{w}_i) + \frac{g}{N}\sum_j \epsilon_{ij}\mathbf{G}(w_j). \tag{1.23}$$

where we have rescaled for clarity the coupling term by the network size N. In the case of Equation (1.23) this choice is useful when the network connectivities scale as the size N of the network, i.e. a massive network. We want the coupling term to remain finite in the thermodynamic limit and comparable at different sizes. If we are dealing with sparse networks it is more convenient to rescale by the average connectivity $\langle k_{in}\rangle$ in order to maintain the coupling term to remain finite.

In this thesis we want to refer to real neural systems that are always finite, i.e. N is a finite number. By considering the dynamics of a certain brain region, we will deal with a specific network of a certain size N with its own network structure. Therefore, a real network is neither massive or sparse and, in the model describing that specific network, the choice of the term $1/N$ or $\langle k_{in}\rangle$ is just a rescaling of the coupling g.

The dynamics of the membrane potential v_i of every node i in a system of N purely excitatory neurons may finally be written in terms of a set of three coupled differential equations:

$$\dot{v}_i = a - v_i + \frac{g}{N}\sum_j \epsilon_{ij} y_j \tag{1.24}$$

$$\dot{y}_i = -\frac{y_i}{\tau_{in}} + U\,(1 - y_i - z_i)S_i \tag{1.25}$$

$$\dot{z}_i = \frac{y_i}{\tau_{in}} - \frac{z_i}{\tau_r} \tag{1.26}$$

where we suppose that the proportional factor c in Equation (1.14) between the active resources y_i and the post-synaptic current between neurons is the same for every couple of neurons [4].

These results represent a model for the dynamics of a population of excitatory neurons (extendable to the inhibitory case) developed by Tsodyks, Uziel and Markram, named TUM model [67]. Physiological parameter values are $\tau_{in} = 0.2$, $\tau_r = 26.6$, $U = 0.5$ for excitatory postsynaptic neurons, and $g = 30$ (but in this thesis, we shall consider the behaviour of this model varying the parameters g and τ_{in}). In the rest of this thesis we will call TUM model the model for short–term plasticity in purely excitatory systems.

1.3.3 Degree-based Mean Field approximation (DMF)

In this section we discuss how to describe the finite size dynamics of the model discussed in Section 1.3.2 through a mean field approximation. Real neural networks (e.g.those producing the fields one usually measures in laboratories) are made of a finite number of elements, whose dynamics we aim to analyze.

The method hereafter reported is based on a mean field approximation and is very general, making it applicable to a wide range of dynamical models on extended structures. We show its implementation in a simple case of excitatory network in spiking regime, where disorder is present only on the network structure. This simple setup has been shown to reproduce non trivial synchronization patterns with the emergence of oscillations in global fields [13]. The mean field model we will obtain permits a deeper understanding of the role of the network structure.

Let us consider a finite size sample made of N neurons connected through a random uncorrelated network. Given a single sample, i.e. let us imagine a real group of neurons, one can define the distribution of specific in degrees $P(k_{in})$ as the envelope of the histogram ideally obtained from the finite size sample with adjacency matrix ϵ_{ij}. The dynamics of the model can then be obtained by integrating Equations (1.25).

A possible way to investigate the dynamics is to perform the thermodynamic limit: an easier analytical treatment and a more performant computer simulation protocol are expected. This approach involves the abstract construction of networks with increasing size. The construction needs to be done in such way that the dynamics of the network at every sufficiently large size N maintains the same features.

A crucial ingredient for the microscopic organization of neurons (and therefore for the dynamics of the system) is the disorder in the connectivity. One can expect that what really matters is not the absolute connectivity k_{in} but the fluctuations of the relative connectivity $\frac{k_{in}}{\langle k \rangle}$. For the construction of network at increasing size we will consider massive networks for which the average connectivity scales as the size N. We will see that in the framework we will consider this is a very general construction as the case with $\langle k \rangle$ constant will be considered a simple rescaling of the

[4] In general, real systems are composed by a relatively small fraction of inhibitory neurons. Experimental observations show that between pyramidal excitatory neurons and inhibitory inter–neurons another mechanism in addition to the depressive one is present in synapses. This mechanism is called facilitation and can be introduced by increasing the synapses efficiency at every spike. We will not consider this kind of mechanisms in this thesis.

coupling among neurons. Accordingly, the parameter whose distribution needs to be maintained in order to observe similar dynamical features is the specific connectivity

$$k = \frac{k_{in}}{N}. \tag{1.27}$$

A possible way to construct a class of networks with the same distribution $P(k)$ is the following. For every neuron i its specific connectivity k_i is extracted from the distribution $P(k)$ and then Nk_i presynaptic neurons are assigned randomly. Notice that the distribution $P(k)$ takes values for $k \in (0, 1]$ and has to be normalized.

In summary, given a reference sample with its own distribution $P(k)$, one needs to construct networks at increasing sizes keeping fixed $P(k)$. In this way, it is possible to preserve the dynamics from a quantitative and a qualitative point of view, apart from statistical fluctuations.

The network construction described preserves the dynamics of the system at each size N. This is true in particular in the thermodynamic limit, i.e. $N \gg 1$. The dynamics of the model in this limit can be a addressed through an approximation based on the finite size fluctuations vanishing in this limit.

In particular, let us consider a neuron i in the ideal infinite structure, characterized by the distribution $P(k)$ of the finite sample of reference. The field Y_i received by this neuron is

$$Y_i(t) = \frac{1}{N} \sum_j \epsilon_{ij} y_j(t) \tag{1.28}$$

In the thermodynamic limit, as the network is massive, the connectivity k_i goes to infinity and, given the randomness of the network (i.e. the choice of presynaptic neurons j is random) one can assume that

$$\frac{1}{k_i} \sum_j \epsilon_{ij} y_j(t) \to \frac{1}{N} \sum_j y_j = Y(t) \tag{1.29}$$

in the limit $N \gg 1$.

Accordingly, by combining Equations (1.28) and (1.29) we find that, in the thermodynamic limit, the field received (apart from the coupling factor g) by every neuron i is

$$Y_i = k_i Y. \tag{1.30}$$

For finite but large values of the connectivity of neurons Equation (1.29) is an approximation equivalent to consider that the average of a large but finite number of fields chosen randomly in the network is approximately equivalent to the average over all neurons in the network. This approximation is valid also when one considers sparse networks and typically a small value of $\langle k \rangle$, compared to the size N of the network, is sufficient [21]. The mean field hypothesis permits to forget about the detail of the network structure, i.e. which neurons fire to the reference neuron i.

In order to determine the dynamics of neuron i it is sufficient to know its specific connectivity k_i. Accordingly, we can write a dynamical equation for the class of

neurons sharing the same specific connectivity k. The evolution equations for each class k_i, that we will use in the rest of this thesis, read:

$$\dot{v}_i(t) = a - v_i(t) + g\, k_i\, Y(t) \tag{1.31}$$

$$\dot{y}_i(t) = -\frac{y_k(t)}{\tau_{in}} + U(1 - y_i(t) - z_i(t))S_i(t) \tag{1.32}$$

$$\dot{z}_i(t) = \frac{y_k(t)}{\tau_{in}} - \frac{z_k(t)}{\tau_r}, \tag{1.33}$$

where v_i, y_i and z_i are the membrane potential, fraction of active and inactive resources of the class of neurons with in–degree k_i, respectively and the mean field $Y(t)$ needs to be consistently written in order to sum over all the microscopic fields y_i weighted for the fraction $P(k)\,dk$ of neurons present in that specific class:

$$Y(t) = \int_0^1 P(k_i) y_i(t) dk_i. \tag{1.34}$$

Notice that k is a continuous variable in the interval $(0, 1]$ and the infinite set of equations (1.31-1.33) is the mean field model relative to a finite size sample characterized by the distribution $P(k)$. This model is said Degree based Mean Field (DMF) and it has to be stressed that it has been constructed in such a way that it keeps track of the inhomogeneity present in finite size realization.

Despite this set of Equations (1.31-1.33) cannot be solved explicitly, they provide a great numerical advantage with respect to direct simulations of large systems. Actually, the basic features of the dynamics of such systems can be effectively reproduced (with loss of finite–size corrections) by exploiting a suitable sampling of $P(k)$. One can subdivide the support (0, 1] of k by M values $k_i (i = 1, \ldots, M)$, in such a way that

$$\int_{k_i}^{k_{i+1}} P(k) dk \tag{1.35}$$

is constant (this procedure is named *importance sampling*). Notice that the integration of the discretized DMF equations is much less time consuming than the simulations performed on a random network.

Part II

Results: Complex Emergent Dynamics

Chapter 2

Mean Field neural network

Networks of spiking neurons feature a wide range of dynamical collective behaviors, that are believed to be crucial for brain functioning [71]. Next to uncorrelated and asynchronous dynamics, quasi-synchronous phases and regimes of irregular activity have been observed, showing a still unexplained degree of correlation that could encode part of the neural function [33, 62, 73, 19, 32, 59]. Understanding the mechanisms that generate such experimentally observed collective behaviours and the transition between them is a major goal in theoretical neuroscience [71, 1, 69, 35, 12, 39, 51, 30, 55].

Interestingly, in cortical networks, irregular activity at the collective level has been widely observed both *in vitro* and *in vivo* [14, 46]. Several mechanisms leading to irregular dynamics in networks of spiking neurons have been proposed. Irregular dynamical phases have been related to a balance between excitatory and inhibitory inputs [4, 70] or to a disorder in the network or in the couplings [12, 17] as crucial ingredients.

In this chapter we show that correlated irregular dynamics can be observed in homogeneous deterministic networks of N identical purely excitatory spiking neurons endowed with synaptic plasticity, coupled by an all to all, mean field (MF), interaction. In this case, all neurons are synchronized but, for small enough synaptic decay time, the system displays a period-doubling transition from a periodic to a chaotic phase. Such a transition can be analytically described by studying the competition among the system timescales in the strong and weak coupling limits, and, in the limit of vanishing synaptic decay time, by reducing the dynamics to a one dimensional map.

The MF case corresponds to considering, in Equations (1.31-1.33) the simple in-degree distribution

$$P(k_i) = \delta(k_i - k_0), \tag{2.1}$$

i.e. the in-degree k_0 (and therefore the coupling constant) is the same for all sites. In this framework each neuron evolves according the same equations and the system is exactly synchronized [23]. Accordingly, the mean field equations reduce to the

dynamics of a single neuron representing the entire system:

$$\begin{aligned} \dot{v}(t) &= a - v(t) + gk_0 y(t) \\ \dot{y}(t) &= -\frac{y(t)}{\tau_{in}} + u(1 - y(t) - z(t))S(t) \\ \dot{z}(t) &= \frac{y(t)}{\tau_{in}} - \frac{z_i(t)}{\tau_R}. \end{aligned} \tag{2.2}$$

where, as discussed in the previous Chapter, v is the membrane potential of the unique neuron present in the MF case (an arbitrary number of neurons exactly synchronizes in this set up, allowing for a sharp dimensional reduction of the dynamics), the y are the active resources propagating the incoming current through the synaptic cleft and z are the inactive (or used) resources. As for the parameters, g is the coupling constant between neurons, u is the synaptic activation constant indicating for the intensity of the spikes, τ_{in} is the inactivation time scale of active resources y_i and τ_R is the recovering time scale of synaptic resources z into recovered ones x. $S(t) = \sum_n \delta(t - t_n)$ is the synaptic spike train, where the t_n are the times of firing events.

The dynamics can be rewritten as a simple event driven map in z_n and y_n, representing the inactive and active resources before the n-th firing event:

$$y_{n+1} = e^{-\frac{\Delta_n}{\tau_{in}}}(y_n + u(1 - y_n - z_n)) \tag{2.3}$$

$$\begin{aligned} z_{n+1} &= -e^{-\frac{\Delta_n}{\tau_{in}}} \frac{y_n + u(1 - y_n - z_n)}{1 - \tau_{in}/\tau_R} \\ &\quad + e^{-\frac{\Delta_n}{\tau_R}} \left(z_n + \frac{y_n + u(1 - y_n - z_n)}{1 - \tau_{in}/\tau_R} \right), \end{aligned} \tag{2.4}$$

where the time interval Δ_n between the n-th and the $(n+1)$-th firing event is obtained from Equation:

$$\begin{aligned} 1 &= a - e^{-\frac{\Delta_n}{\tau_{in}}} \frac{g\tau_{in}k_0(y_n + u(1 - y_n - z_n))}{1 - \tau_{in}} \\ &\quad - e^{-\Delta_n} \left(a - \frac{g\tau_{in}k_0(y_n + u(1 - y_n - z_n))}{1 - \tau_{in}} \right). \end{aligned} \tag{2.5}$$

where we take into account that the single neuron fires at each event, and therefore we have imposed in equation (2.5) that

$$v_n = 0. \tag{2.6}$$

For all practical purposes, the implicit solution of the first of Equations (2.5) is used to obtain the firing time intervals Δ_n. The spiking time of neurons may be calculated up to machine precision by solving the implicit Equation (2.5) numerically with a bisection procedure, or by means of other numerical methods. The other two Equations (2.3) and (2.4) represent a discrete two dimensional map for the variables y_n and z_n.

2.1 Competition of time-scales

Considering the synaptic time-scales τ_{in} and τ_R and the period of the free neuron

$$T = \ln\left(\frac{a}{a-1}\right) \tag{2.7}$$

and imposing among them the relation

$$\tau_{in} \ll T \ll \tau_R, \tag{2.8}$$

an insight on the dynamics can be achieved by considering the opposite regimes of weak and strong interaction, i.e. when

$$gk_0 y(t) \tag{2.9}$$

or

$$a - v(t) \tag{2.10}$$

are negligible in the first of Equations (2.2), respectively. In both extreme regimes, the map in Equations (2.3 - 2.5) can be solved and has a periodic fixed point solution as will be shown. In particular, in the weak coupling regime, the periodicity is trivially T, and the interaction term remains negligible if

$$gk_0\tau_{in} \ll \frac{\tau_R}{T}. \tag{2.11}$$

On the other hand, if the

$$a - v_{k_0}(t) \tag{2.12}$$

term can be ignored, the system (2.3 - 2.5) displays a much faster periodicity:

$$T_f = \frac{\tau_R}{gk_0\tau_{in}} \tag{2.13}$$

and the approximations holds only if

$$gk_0\tau_{in} \gg a\frac{\tau_R}{\tau_{in}}. \tag{2.14}$$

According to the above discussion, in the MF TUM model we have, for small enough τ_{in},

$$g_c^{weak} \ll g_c^{strong}. \tag{2.15}$$

We therefore expect three different regimes: for small and large values of g a slow and a fast periodic dynamics should be present, while in an intermediate wide range of the synaptic couplings

$$g_c^{weak} \ll g \ll g_c^{strong} \tag{2.16}$$

the competition of the two mechanisms could give rise to a complex dynamics.

The single neuron MF Equations (2.2, 2.3-2.5) become particularly simple in the weak-coupling and strong-coupling regimes. In the former, we can neglect the term

$$gk_0 y(t) \tag{2.17}$$

in Equations (2.2) while in the latter we neglect

$$a - v(t). \tag{2.18}$$

In both limits, the map (2.3 - 2.5) has a fixed point, characterized by a slow and a fast periodicity respectively.

Let us first discuss some general property of the fixed point. We consider the regime

$$T = \ln\left(\frac{a}{a-1}\right) \sim O(1) \tag{2.19}$$

and

$$\tau_{in} \ll T \ll \tau_R, \tag{2.20}$$

so that the event driven dynamics (2.3-2.5) of the MF model becomes:

$$1 = a - g\tau_{in}k_0 y_{n+1} - e^{-\Delta_n}\left(a - g\tau_{in}k_0(y_n + u(1-y_n-z_n))\right) \tag{2.21}$$

$$y_{n+1} = e^{-\frac{\Delta_n}{\tau_{in}}}\left(y_n + u(1-y_n-z_n)\right) \tag{2.22}$$

$$z_{n+1} = -y_{n+1} + e^{-\frac{\Delta_n}{\tau_R}}\left(y_n + z_n + u(1-y_n-z_n)\right). \tag{2.23}$$

We denote with

$$(x^*, y^*) \tag{2.24}$$

the fixed point of the map (2.21-2.23) and with Δ^* the relevant interspike interval, i.e. Equations (2.21-2.23) are satisfied by

$$y_{n+1} = y_n = y^* \tag{2.25}$$

$$x_{n+1} = x_n = x^* \tag{2.26}$$

$$\Delta_{n+1} = \Delta_n = \Delta^*. \tag{2.27}$$

Equations (2.22-2.23) hold both in the strong and in the weak coupling regimes and they describe a general property of the fixed point. In particular, considering the variable

$$w^* = y^* + z^*, \tag{2.28}$$

Equation (2.23) reads:

$$w^* = e^{-\frac{\Delta^*}{\tau_R}}\left(w^* + u(1-w^*)\right) \tag{2.29}$$

and, using the initial assumption:

$$\Delta^* \ll \tau_R. \tag{2.30}$$

Equation (2.29) may be rewritten as:

$$w^* = u\frac{e^{-\frac{\Delta^*}{\tau_R}}}{1-(1-u)e^{-\frac{t^*}{\tau_R}}} \simeq 1-\frac{\Delta^*}{u\tau_R}, \tag{2.31}$$

Inserting Equation (2.31) in Equation (2.22), the equation for the fixed point of y^* reads:

$$y^* = \frac{\Delta^*}{\tau_R}\frac{e^{-\frac{\Delta^*}{\tau_{in}}}}{1-e^{-\frac{\Delta^*}{\tau_{in}}}}. \tag{2.32}$$

Let us come back to the differential equations (2.2) and consider the periodic solution corresponding to the fixed point of the map. Since y^* represent the value of $y(t)$ immediately before a firing event, if we set the time axes so that the firing events occur at

$$t = 0,\ \Delta^*,\ 2\Delta^*,\ ..., \tag{2.33}$$

for $0 < t < \Delta^*$ we have that:

$$y(t) = \frac{\Delta^*}{\tau_R}\frac{e^{-\frac{t}{\tau_{in}}}}{1-e^{-\frac{\Delta^*}{\tau_{in}}}}. \tag{2.34}$$

We remark that, at the fixed point, the above dynamical evolution holds for any value of the coupling constant. However, the value of Δ^* is determined by Equation (2.21) which explicitly depends on g. In particular, in the strong coupling regime Equation (2.21) reduces to:

$$1 = -g\tau_{in}k_0 y_{n+1} + g\tau_{in}k_0(y_n + u(1-y_n-z_n)). \tag{2.35}$$

Imposing now:

$$y^* = y_{n+1} = y_n \tag{2.36}$$
$$z^* = z_{n+1} = z_n \tag{2.37}$$

we get

$$1 = g\tau_{in}k_0 u(1-y^*-z^*), \tag{2.38}$$

which gives the expansion for the fixed point value of w^*:

$$w^* = 1 - \frac{1}{uk_0 g\tau_{in}}. \tag{2.39}$$

Comparing Equation (2.31) with Equation (2.39) we get:

$$\Delta^* = \Delta^*_S \simeq \frac{\tau_R}{g\tau_{in}k_0}. \tag{2.40}$$

On the other hand, in the weak coupling regime, we obviously obtain

$$\Delta^* = \Delta^*_W = \ln\left(\frac{a}{a-1}\right) \simeq O(1). \tag{2.41}$$

We now plug (2.34) into the first of Equations (2.2), describing the evolution of the membrane potentials, and we verify under which conditions the periodicity of the weak and strong coupling regime remains unperturbed. In particular, for

$$0 < t < \Delta^*, \tag{2.42}$$

we have that the membrane potential $v(t)$ satisfies the equation:

$$\dot{v}(t) = a - v(t) + \frac{gk_0\Delta^*}{\tau_R} \frac{e^{-\frac{t}{\tau_{in}}}}{1 - e^{-\frac{\Delta^*}{\tau_{in}}}}. \tag{2.43}$$

where Δ^* is the time relative to the periodic solution for the membrane potential v. Solving the differential equation and imposing

$$\tau_{in} \ll 1, \tag{2.44}$$

we get:

$$v(t) = a(1 - e^{-t}) + \frac{g\tau_{in}k_0\Delta^*}{\tau_R} \frac{1}{1 - e^{-\Delta^*/\tau_{in}}} \left(e^{-t} - e^{-\frac{t}{\tau_{in}}} \right). \tag{2.45}$$

Now we need to verify under which conditions on g, in the weak and strong coupling regime, the solution of

$$v(t^*) = 1, \tag{2.46}$$

that implicitly gives the period of evolution of the neuron and therefore the spiking times, remains close to

$$t^* = \Delta^*_W \tag{2.47}$$
$$t^* = \Delta^*_S, \tag{2.48}$$

where Δ^*_W and Δ^*_S are the period of evolution of the membrane potential v in the weak and strong coupling limit, respectively.

2.1.1 Weak coupling

For small g, we have that the periodicity Δ^*_W and the evolution time are much larger than τ_{in}, therefore Equation (2.45) can be written as:

$$v(t) \simeq a(1 - e^{-t}) + \frac{g\tau_{in}k_0\Delta^*_W}{\tau_R} e^{-t} \tag{2.49}$$

solving $v(t^*) = 1$ we get

$$t^* \simeq \ln\left(\frac{a - g\tau_{in}k_0\Delta^*_W}{\tau_R\,(a-1)} \right) \tag{2.50}$$

and then:

$$t^* \cong \Delta^*_W = \ln\left(\frac{a}{a-1} \right) \tag{2.51}$$

only if

$$\frac{g\tau_{in}k_0\Delta^*}{\tau_R} \ll 1, \tag{2.52}$$

i.e. the periodicity of the weak coupling regime is preserved if

$$g \ll g_c^{weak} \tag{2.53}$$

with:

$$g_c^{weak} = \frac{\tau_R}{\tau_{in}k_0 \ln(\frac{a}{a-1})}. \tag{2.54}$$

2.1.2 Strong coupling

In this case we have that the period Δ_S^* and the evolution time t are much smaller than

$$T \simeq O(1). \tag{2.55}$$

Therefore, we can approximate Equation (2.45), so that:

$$v(t) \simeq at + \frac{1 - e^{-\frac{t}{\tau_{in}}}}{1 - e^{-\frac{\Delta_S^*}{\tau_{in}}}}. \tag{2.56}$$

Let us discuss Equation (2.56) considering the two opposite regimes

$$\Delta_S^* \ll \tau_{in} \tag{2.57}$$

and

$$\Delta_S^* \gg \tau_{in} \tag{2.58}$$

For $\Delta_S^* \ll \tau_{in}$ also $t \ll \tau_{in}$ and we can expand Equation (2.56) obtaining:

$$v(t) \simeq at + \frac{t}{\Delta_S^*} \tag{2.59}$$

and since

$$\Delta_S^* \ll \tau_{in} \ll a^{-1}, \tag{2.60}$$

the solution of $v(t^*) = 1$ is

$$t^* \simeq \Delta_S^*. \tag{2.61}$$

In the opposite limit, i.e. $\Delta_S^* \gg \tau_{in}$, we have

$$e^{-\Delta_S^*/\tau_{in}} \simeq 0 \tag{2.62}$$

and Equation (2.56) can be approximated as:

$$v(t) \simeq at + 1 - e^{-\frac{t}{\tau_{in}}}. \tag{2.63}$$

Now $v(t^*) = 1$ implies that

$$at^* \simeq e^{-\frac{t^*}{\tau_{in}}} \tag{2.64}$$

so that the firing time is of the same order of magnitude of τ_{in}; this means that

$$t^* \simeq \tau_{in} \ll \Delta_S^*. \tag{2.65}$$

Therefore, in the full dynamics we obtain a self consistent solution

$$t^* \simeq \Delta_S^* \tag{2.66}$$

which can be considered a perturbation of the strong coupling periodic evolution only for the case $\Delta_S^* \ll \tau_{in}$, i.e. only if

$$g \gg g_c^{strong} \tag{2.67}$$

with

$$g_c^{strong} = \frac{\tau_R}{k_0 \tau_{in}^2}. \tag{2.68}$$

In this Section, by neglecting in the first of Equations (2.2) for the evolution of the membrane potential v the terms relative to the connection to other neurons in the limit of weak coupling, and the term corresponding to periodic free evolution in the strong coupling one, we have found the critical value of the coupling constant that is required in order to find consistently the weak or the strong coupling limit, i.e. (2.54) and (2.68) respectively.

2.2 Transition to chaos in the Mean Field model

In this section we will see that the presence of a further non trivial phase may be put in evidence by considering the fully MF case. All neurons become completely synchronized after an initial transient state, as can be verified numerically. We recall that Equations (2.2) are the reduced equations of a single neuron with coupling k_0.

As we have seen in the previous section, in the region of the parameters

$$\frac{\tau_R}{T} \ll g k_0 \tau_{in} \ll \frac{\tau_R}{\tau_{in}}, \tag{2.69}$$

neither the weak nor the strong coupling conditions are satisfied, and the competition between local and interacting terms, with slow or fast periodicity, plays a non trivial role destroying the presence of a periodic evolution. Such a behavior can be analyzed by means of the bifurcation diagram of the inter-time interval Δ_n as a function of the synaptic coupling g at fixed value of the synaptic time-scale τ_{in}.

Figure 2.1 shows the presence of a stable fixed point for small and large values of g, describing the slow and a fast periodic regime, respectively. For an intermediate value, a period doubling first appears, then, at a critical value g' t.c.:

$$g > g'(\tau_{in}), \tag{2.70}$$

the distribution of Δ_n becomes continuous. The Δ_n becomes again delta-distributed for

$$g > g''(\tau_{in}). \tag{2.71}$$

The critical values of both g and τ_{in} depend on the value of a (the intrinsic period of the neuron) and a chaotic dynamics is observed at higher τ_{in} values by considering smaller a.

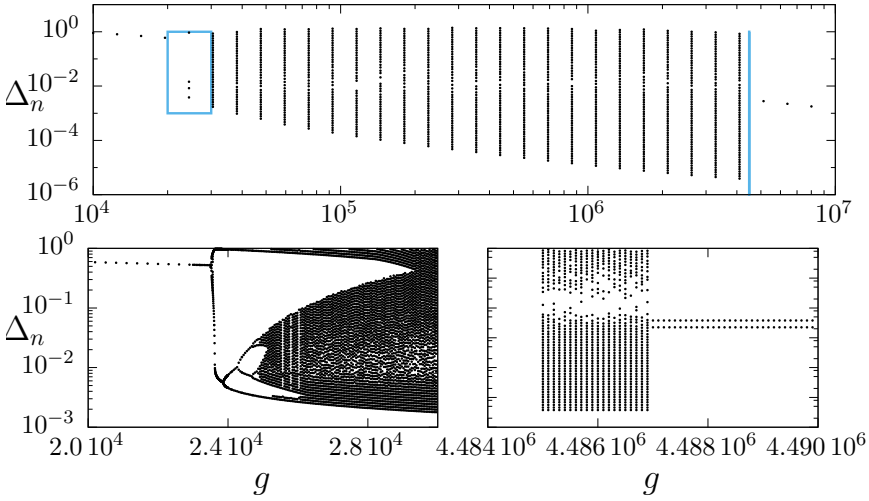

Figure 2.1. Feigenbaum bifurcation diagram for the MF TUM model described by Equations (2.3-2.4) with $\tau_{in} = 10^{-3}$. The attractor for the interspike interval of the network Δ_n is showed as a function of the coupling constant g. Upper panel: bifurcation diagram in the full relevant range of the bifurcation parameter g. Lower-left panel: magnification on the period doubling cascade at the first transition. Lower-right panel: magnification on the second transition. The blue rectangles in the upper panel indicate the zooming regions corresponding to the lower panels.

We show respectively in Figures 2.2 and 2.3, for the MF model, the bifurcation diagrams of the temporal difference

$$\Delta_n \equiv t_{n+1} - t_n \tag{2.72}$$

between two consecutive spikes of the network as a function of g for different values of τ_{in}, and the analogous values of the *coefficient of variation* CV, defined by the standard deviation of the interspike interval Δ_n over its mean:

$$CV = \frac{\sigma_{\Delta_n}}{\langle \Delta_n \rangle}. \tag{2.73}$$

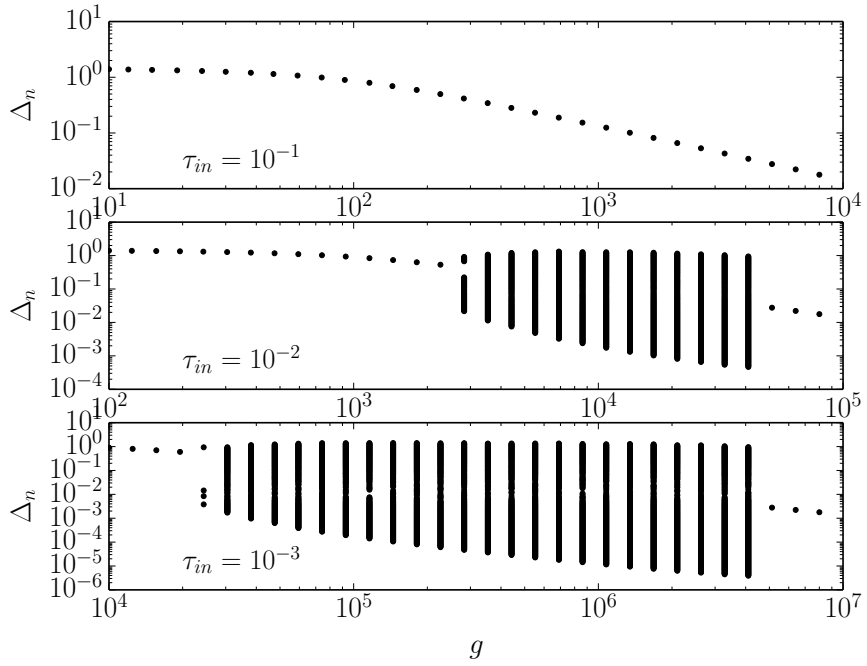

Figure 2.2. Feigenbaum bifurcation diagram for the MF TUM model with $\tau_{in} \neq 0$. The attractor for the interspike interval Δ_n is showed as a function of the bifurcation parameter, i.e. the coupling constant g. The bifurcation diagram is shown for decreasing values of the synaptic time scale τ_{in} from the top panel to the lower ($\tau_{in} = 10^{-1,-2,-3}$ respectively) in order to show the appearance and growth of the chaotic regime in the parameter space (notice that the x-axis range is different for each panel).

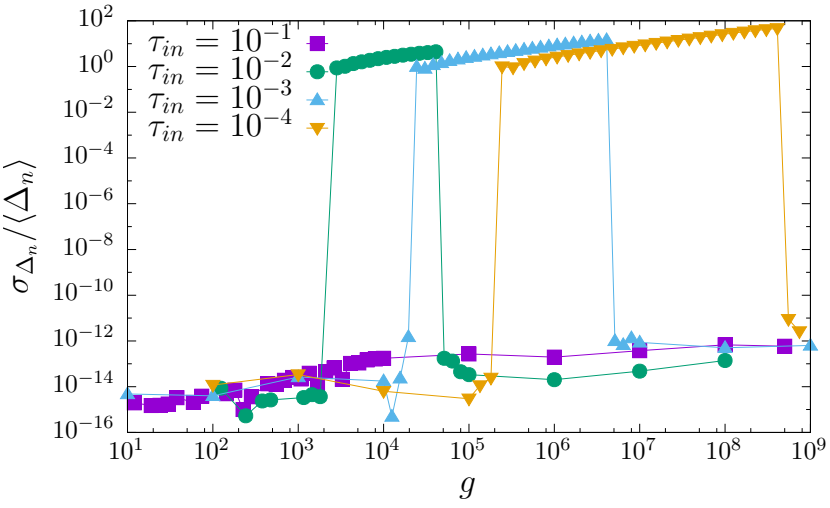

Figure 2.3. Coefficient of Variation of the interspike interval, $\frac{\sigma_{\Delta_n}}{\langle\Delta_n\rangle}$, for several values of τ_{in}. This quantity is of order 1 in the chaotic regime only.

In Figure 2.4 we report a raster plot showing that the system converges in the MF case (where $k_i = k_0$ for all sites), after a short transient, to a synchronous state

where all neurons fire simultaneously. This had already been observed in a parameter setup showing periodic synchronous dynamics [23]. Nevertheless, in the present case the synchronous solution shows an irregular chaotic dynamics, indicating our system as an example of synchronous chaos [24, 31]. Since each neuron displays the same dynamical evolution, the assumption that the MF equations reduce to the dynamics of a single neuron representing the entire system is justified in all the phases the system undergoes.

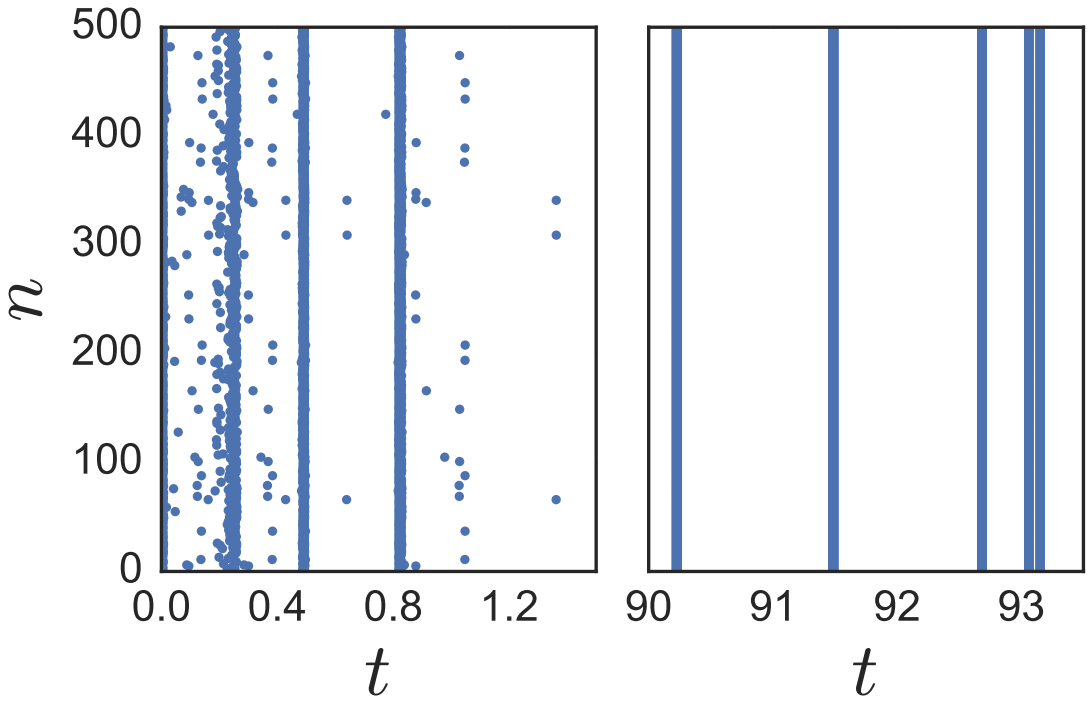

Figure 2.4. Raster plot of a fully MF system with $k_i = k_0 = 0.7$, $g = 10^6$ $\tau_{in} = 10^{-3}$. Each dots represent the firing event of neuron n. Left: short time evolution. Right: long time evolution the system reach a synchronous but chaotic state.

The numerical calculation of the Lyapunov exponents (via the Gram-Schmidt scheme [8, 61]) in the N neurons MF model confirms the presence of the chaotic regime in the range of the parameter g between the two bifurcations, as shown in Figure 2.5. In this region the maximum Lyapunov exponent λ_1 becomes positive. Analogous figures can be obtained for other values of τ_{in}.

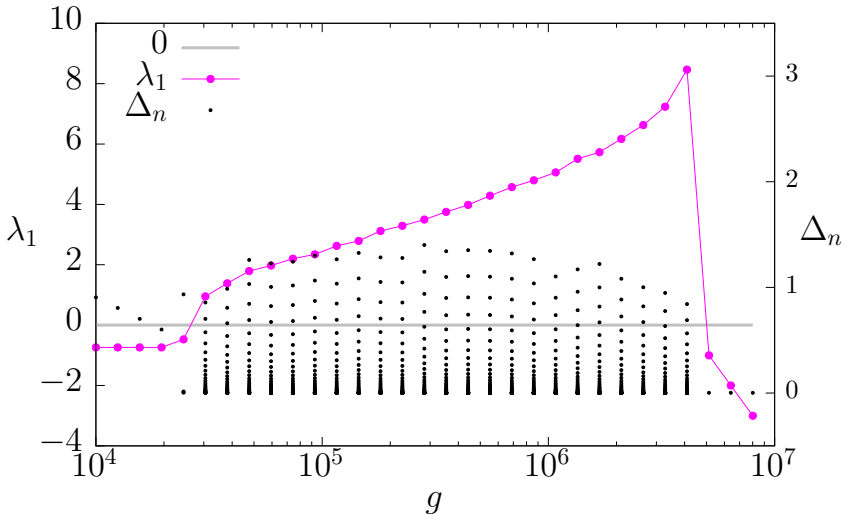

Figure 2.5. First Lyapunov exponent λ_1 (in red) as a function of g for the MF TUM model with $\tau_{in} = 10^{-3}$. In black, for comparison: bifurcation diagram as a function of g for the same model (right x-axis). The sign of the first Lyapunov exponent λ_1 confirms a chaotic regime ($\lambda_1 > 0$) between the synchronous-bursty and bursty-asynchronous transitions outside this region ($\lambda_1 < 0$).

2.3 The limit $\tau_{in} \to 0$: the simplest dynamics

Considering the MF dynamical equations (2.3-2.5) in the limit

$$\tau_{in} \to 0,\ g \to \infty \ \text{ with } \ g\tau_{in} = \text{const.}, \tag{2.74}$$

so that the new effective coupling constant is defined by

$$g_{\text{eff}} = k_0 g \tau_{in} \tag{2.75}$$

in Equations (2.3-2.5), we obtain a single variable map as a function of

$$g_{\text{eff}},\ a \ \text{ and } \ \tau_R \tag{2.76}$$

only, that can be studied analytically as we will see in this section. Without loss of generality we consider

$$k_0 = 1 \tag{2.77}$$

in the following. This simpler map confirms the presence of a true chaotic dynamical phase.

Let us reintroduce the two notations:

$$x = 1 - y - z \tag{2.78}$$
$$x_n = 1 - y_n - z_n \tag{2.79}$$

where x_n are the available resources before the n-th firing event. If

$$g_{\text{eff}}(y_n + u x_n) < 1 \tag{2.80}$$

the evolution time Δ_n after the n-th firing event is larger than zero and, in particular, from Equation (2.5) we obtain:

$$\Delta_n = \ln\left(\frac{a-1}{a - g_{\text{eff}}(y_n + ux_n)}\right) > 0. \tag{2.81}$$

Then, taking the limit $\tau_{in} \to 0$ in Equations (2.3 - 2.5) we get

$$y_{n+1} = 0 \tag{2.82}$$
$$x_{n+1} = 1 + (x_n(1-u) - 1)e^{-\Delta_n/\tau_{\text{R}}} \tag{2.83}$$

which is a discrete map counterpart of the differential equation:

$$\dot{x}(t) = \frac{1 - x(t)}{\tau_R} - ux(t)\sum_m \delta(t - t_{n+1}(m)). \tag{2.84}$$

Therefore, if $g_{\text{eff}}(y_n + ux_n) < 1$, we reduce to a single variable map for x_n, obtained inserting the expression for Δ_n (2.81) into Equation (2.83).

On the other hand, if

$$g_{\text{eff}}(y_n + ux_n) > 1 \tag{2.85}$$

the solution of Equation (2.5) can be obtained letting also

$$\Delta_n \to 0 \text{ with } \frac{\Delta_n}{\tau_{\text{in}}} = \text{const.}, \tag{2.86}$$

so we get

$$1 = -g_{\text{eff}}\left(e^{-\Delta_n/\tau_{\text{in}}} - 1\right)(y_n + u(1 - y_n - z_n)) \tag{2.87}$$

or:

$$e^{-\Delta_n/\tau_{\text{in}}} = \frac{g_{\text{eff}}(y_n + ux_n) - 1}{g_{\text{eff}}(y_n + ux_n)}. \tag{2.88}$$

Plugging (2.88) into Equation (2.3) we have:

$$y_{n+1} = y_n + ux_n - \frac{1}{g_{\text{eff}}} \tag{2.89}$$

Taking the limits $\tau_{\text{in}} \to 0$ and $\Delta_n \to 0$ in Equation (2.4):

$$z_{n+1} = -y_{n+1} + (z_n + y_n + u(1 - y_n - z_n)) \tag{2.90}$$

i.e.

$$x_{n+1} = x_n(1-u) \tag{2.91}$$

as it is expected in an instantaneous firing event.

In conclusion, if $g_{\text{eff}}(y_n + ux_n) < 1$, the evolution time Δ_n is given by (2.81), $y_{n+1} = 0$ and x_{n+1} is given by Equation (2.83). If

$$g_{\text{eff}}(y_n + ux_n) > 1 \tag{2.92}$$

the evolution is instantaneous, $\Delta_n = 0$ and the maps for x_n and y_n are described by Equations (2.89) and (2.91).

In this MF case, the dynamical description can be further summarized introducing two new indexes m and p, labelling the firing events. The label m increases of one unit each time there is a firing event such that $\Delta_n > 0$ and $p = 1 \dots, p_m$ labels the different simultaneous firing events. In this way we replace the index n with the couple (m, p): if in the firing event $\Delta_n = 0$, m remains fixed and p increases by one, while, if $\Delta_n > 0$, m increases by one and p is reset to 1 (p_m is the value of p for which m is increased to $m + 1$ and p is reset). With this new labels for the events, we denote $x_{(p,k)} = x_n$, $y_{(p,k)} = y_n$ and so on.

For a given value of m, from $p = 1$ to $p = p_m$, Equations (2.89) and (2.91) can be easily evaluated obtaining:

$$x_{(m,p)} = x_{(m,1)}(1 - u)^{p-1} \tag{2.93}$$

and

$$y_{(m,p)} = (1 - (1 - u)^{p-1})x_{(m,1)} - \frac{p - 1}{g_{\text{eff}}} \tag{2.94}$$

where Equation (2.94) can be verified recursively taking into account that

$$y_{(m,1)} = 0. \tag{2.95}$$

The number of simultaneous firings p_m can be evaluated by verifying if

$$g_{\text{eff}}(y_{(p,k)} + ux_{(p,k)}) < 1, \tag{2.96}$$

in particular from Equations (2.93) and (2.94) we obtain that p_m is the smallest positive integer such that:

$$gx_{(m,1)}(1 - (1 - u)^{p_m}) - p_m < 0. \tag{2.97}$$

When $p = p_m$ the time evolves of a step $\Delta_{(m,p)}$ given by (2.81):

$$\Delta_{(m,p_m)} = \ln\left(\frac{a - 1}{a - g_{\text{eff}}(y_{(m,p_m)} + ux_{(m,p_m)})}\right) \tag{2.98}$$

$$= \ln\left(\frac{a - 1}{a - g_{\text{eff}}x_{(m,1)}(1 - (1 - u)^{p_m}) + p_m - 1}\right) \tag{2.99}$$

and the resources evolve according to Equation (2.83):

$$\begin{aligned} x_{(m+1,1)} &= 1 + (x_{(m,p_n)}(1 - u) - 1)e^{-\Delta_{(m,p_m)}/\tau_{\text{R}}} \\ &= 1 + (x_{(m,1)}(1 - u)^{p_m} - 1)e^{-\Delta_{(m,p_m)}/\tau_{\text{R}}} \end{aligned} \tag{2.100}$$

Finally we can plug Equation (2.99) into (2.100) obtaining:

$$\begin{aligned} x_{(m+1,1)} = 1 \quad &+ \quad (x_{(m,1)}(1 - u)^{p_m} - 1) \\ &\cdot \left(\frac{a - 1}{a - g_{\text{eff}}x_{(m,1)}(1 - (1 - u)^{p_m}) + p_m - 1}\right)^{1/\tau_R} \end{aligned} \tag{2.101}$$

where p_m is the smallest positive integer satisfying Equation (2.97). Equation (2.101) represents a map for the variable $x_{(m+1,1)}$. The map (2.101) is shown in Figures 2.6 and 2.7 (c.f. captions for details).

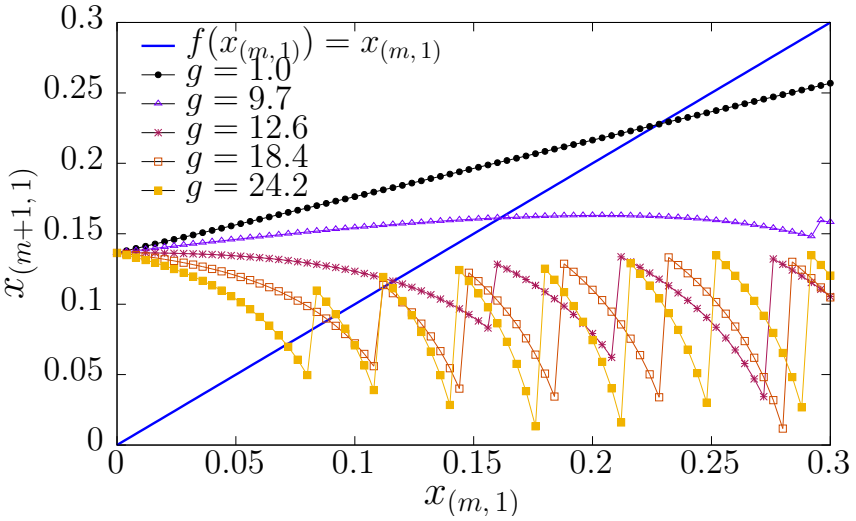

Figure 2.6. Map (2.101) for the MF TUM model with $\tau_{in} = 0$ for different values of g_{eff} indicated in the legend.

For small values of g_{eff} the map exhibits a stable fixed point. Increasing g_{eff}, a stable period–2 orbit is observed (see Figure 2.7). Finally, at larger values of the coupling, typically when the map features two intersections with the bisector $x_{(m+1,1)} = x_{(m,1)}$, the dynamical attractor explores a region of the phase space that cannot be confined in a limit cycle.

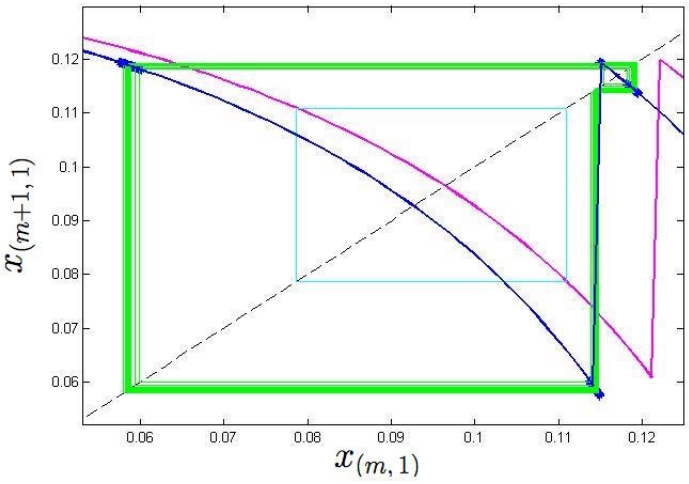

Figure 2.7. In order to highlight the difference between the quasi-synchronous and the bursty transitions, two values of g_{eff} are plotted in both regimes respectively. For $g_{\text{eff}} = 16$ a period-two orbit is observed (light blue), while for $g_{\text{eff}} = 30$ - notice that the discontinuity of the map has crossed the $y = x$ line - a chaotic behavior is present (green).

The disappearance of the limit cycle at large values of the synaptic coupling g is confirmed by the calculation of the invariant measure that presents a broad distribution (see Figure 2.8). We have seen in Section 2.2 that this region is strictly chaotic as the Lyapunov exponent of the map is larger then zero, as soon as the limit cycle loses stability.

We remark that for $\tau_{in} \to 0$ the periodic regime at large values of g does not exist. Indeed, the coupling constant g, for $\tau_{in} \to 0$, diverges as:

$$g \sim \frac{g_{\text{eff}}}{\tau_{in}}, \tag{2.102}$$

while the transition point between the bursty and the asynchronous regimes diverges in the same limit as

$$g \sim g_c^{strong} \sim \tau_{in}^{-2}. \tag{2.103}$$

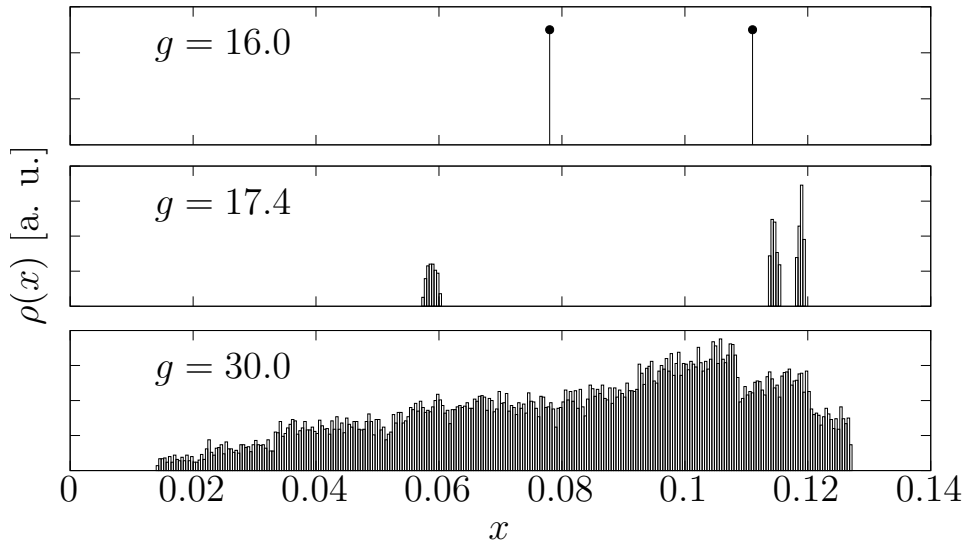

Figure 2.8. Probability density $\rho(x)$ of the synaptic resource x_n, for $g_{\text{eff}} = 16$ (upper panel), $g_{\text{eff}} = 17.4$ (middle panel) and $g_{\text{eff}} = 30$ (lower panel). While two peaks are present for $g_{\text{eff}} = 16$, indicating a period-two orbit, a broad distribution, indicating chaotic dynamics, is observed in the last two cases.

Limit $\tau_{in} \to 0$ in the DMF model

We end this section by noticing that an analogous limit $\tau_{in} \to 0$ can be performed also on the DMF equations obtaining for the dynamical variables $v_i(t)$ and $x_i(t)$ a set of equations similar to the TUM model described in [41]:

$$\dot{v}_i(t) = a - v_i(t) + g\tau_{in} k_i \frac{1}{M} \sum_{j=1}^{M} x_j(t) S_j(t) \tag{2.104}$$

$$\dot{x}_i(t) = \frac{1 - x_i(t)}{\tau_R} - u x_i(t) S_i(t) \tag{2.105}$$

where $g\tau_{in}$ is the new effective coupling constant. Moreover, also in this case simultaneous firing events are possible. In particular, if neuron j fires at time t_m and

$$v_i(t_m) + uM^{-1}x_j(t_m) > 1 \tag{2.106}$$

also neuron i fires at t_m and $v_i(t_m)$ is set to

$$v_i(t_m) + uM^{-1}x_j(t_m) - 1. \tag{2.107}$$

We remark that also in the DMF case, reintroducing the potential variable

$$v_{n+1} = g_{\text{eff}}(y_n + ux_n) \tag{2.108}$$

in Equations (2.89, 2.91), we can eliminate y_n obtaining

$$v_{n+1} = v_n + ug_{\text{eff}}x_n - 1, \tag{2.109}$$

i.e. the natural equation for a neuron that receive an input $ug_{\text{eff}}x_n$ and simultaneously fires decreasing by one unit.

Chapter 3

Degree-based Mean Field Dynamics

A particularly interesting dynamical signature of collective irregular regimes in neural dynamics is the one of *avalanches* or bursts of spiking neurons with heavy-tailed distributions of activity [32, 49, 44]. In cortical networks, avalanches characterized by power-law distributions have been widely observed both *in vitro* and *in vivo* [7, 60, 57, 25]. These regimes are thought to be closely related to information processing in the cortex [38, 54, 52] and to adaptive [15] and healthy [48] behaviour.

Several mechanisms leading to bursts in networks of spiking neurons have been proposed: power-law distributed avalanches have been attributed to synaptic plasticity with a stochastic noise in the charging [42, 10, 9, 50, 72] or to dynamical mechanisms inspired by self-organized criticality (SOC) [18, 15, 20]. The balance between excitation and inhibition has been found to play an important role, analogously to what happens in irregular dynamics, in this bursty dynamical regime [45], and a relation between uncorrelated dynamics in a network of stochastic units and power-law scaling has been proposed [64, 63].

In this chapter we show that in the disordered version of our model endowed with short-term synaptic plasticity, e.g. considering a Degree based Mean Field (DMF) in the couplings, the dynamics exhibits three phases, depending on the interaction strength g and synaptic decay time τ_{in}. In particular, in addition to the quasi periodic and the asynchronous regimes [13], a phase characterized by power-law distributed avalanches emerges in correspondence to the chaotic phase of the homogeneous MF model. Chaos is preserved in this dynamical phase, as confirmed by the computation of the Lyapunov exponents, and it is characterized by the onset of strong temporal correlations and high complexity.

We consider a disordered random network of leaky integrate-and-fire (LIF) neurons [34] connected via the Tsodyks-Uziel-Markram (TUM) model for short term synaptic plasticity [67].

In the Degree Based Mean Field approximation (DMF) [22, 13], that has been shown to reproduce the relevant features of the collective dynamics of this model, neurons (neuron-classes) are labeled by the index $i = 1 \dots N$ (we consider a system of N neurons) and they are characterized by their coupling constant gk_i, randomly extracted from $P(k_i)$, the distribution of couplings in the network. Nk_i can be

interpreted as the effective in-degree of neuron i, so that $P(k_i)$ may also be considered a degree distribution. In this framework, therefore, Nk_i represents the only relevant topological feature of the structure and this justifies the DMF name.

The DMF Equations (1.31-1.33) can be solved by an event-driven map, by means of which numerical simulations of the model can be performed very efficiently [11, 13]. We denote with $v_{i,n}$, $y_{i,n}$, and $z_{i,n}$ the value of $v_i(t_n)$, $y_i(t_n)$ and $z_i(t_n)$ *immediately before the n-th firing event* and with $\Delta_n = t_{n+1} - t_n$ the time interval between the firing events ($t_i(m)$ denotes firing times of neuron i while t_n represents the sequence of firing times of the network, independently of the firing neuron). The evolution of the discrete variables then reads:

$$\begin{aligned} v_{i,n+1} &= v_{i,n}e^{-\Delta_n} + a(1-e^{-\Delta_n}) + \frac{gk_i\tau_{\rm in}}{\tau_{\rm in}-1}\left(e^{-\Delta_n/\tau_{\rm in}} - e^{-\Delta_n}\right)\frac{1}{M}\sum_{j=1}^{M} y_{j,n} \\ y_{i,n+1} &= (y_{i,n} + \delta_{i,s_{n+1}}u(1-y_{i,n}-z_{i,n}))e^{-\Delta_n/\tau_{\rm in}} \\ z_{i,n+1} &= z_{i,n}e^{-\Delta_n/\tau_R} \\ &\quad + \frac{\tau_{\rm R}}{\tau_{\rm R}-\tau_{\rm in}}(y_{i,n} + \delta_{i,s_{n+1}}u(1-y_{i,n}-z_{i,n}))\left(e^{-\Delta_n/\tau_{\rm R}} - e^{-\Delta_n/\tau_{\rm in}}\right) \end{aligned} \tag{3.1}$$

where $\delta_{i,j}$ is the Kronecker delta and s_n is the neuron that fires at time t_n. To implement the reset rule on the potential, for neuron s_{n+1} that fires at t_{n+1} the first Equation (3.1) is replaced by:

$$\begin{aligned} 1 &= v_{s_{n+1},n}\,e^{-\Delta_n} + a(1-e^{-\Delta_n}) \\ &\quad + gk_i\tau_{\rm in}\frac{e^{-\Delta_n/\tau_{\rm in}} - e^{-\Delta_n}}{\tau_{\rm in}-1}\frac{1}{M}\sum_{j=1}^{M}(y_{j,n} + \delta_{j,s_n}u(1-y_{j,n}-z_{j,n})) \end{aligned} \tag{3.2}$$

and $v_{s_{n+1},n+1} = 0$. Notice that Equation (3.2) allows to calculate Δ_n and that the firing neuron is identified by finding the value of s_{n+1} that provides the minimum value of Δ_n in Equation (3.2).

Analogously to the MF case, Equations (3.1) are characterized by three time scales: the period of the oscillating non interacting neuron $T = \log(a/(a-1))$, the recovery time τ_R and the synaptic decay time τ_{in}. In the DMF set-up, the regime

$$\tau_{in} \lesssim T \tag{3.3}$$

has been studied in detail in [23], and it features a transition from a quasi-synchronous to an asynchronous phase as a function of g and of the shape of the coupling distribution $P(k_i)$.

Here we will focus instead on the regime

$$\tau_{in} \ll T \ll \tau_R, \tag{3.4}$$

setting $a = 1.3$, $\tau_R = 10$ and varying τ_{in} between 10^{-1} and 10^{-5}. These parameter values are consistent with those selected in [67], where they have been chosen on the basis of biological motivations [1].

[1] See Appendix B for a thorough discussion on this subject.

3.1 Persistence of the chaotic regime and order parameters

Let us consider the multi-site DMF model with heterogeneous couplings extracted from a generic distribution $P(k_i)$. Most of the numerical results presented in this chapter correspond to a Gaussian $P(k_i)$ with mean $\mu = 0.7$ and variance $\sigma = 0.077$. We recall that we are referring to k_i as the normalized in-degree, $k_i = \frac{k_{in}}{N} \in [0; 1)$, such that the in-degree is $k_{in} = N \cdot k_i$.

A relevant quantity describing the dynamical evolution and in particular the synchronicity level of the neurons is the Kuramoto parameter, which measures the synchronization level of a network of dynamical units: [3]:

$$R(t) = \frac{1}{N} \left| \sum_{i=1}^{N} \mathrm{e}^{\imath \phi_i(t)} \right|$$

where $\phi_i(t)$ is the phase of neuron i at time t:

$$\phi_i(t) = 2\pi \frac{t - t_i(m)}{t_i(m+1) - t_i(m)}, \tag{3.5}$$

and $t_i(m)$ is the m-th spike of neuron i and

$$t \in [t_i(m),\, t_i(m+1)]. \tag{3.6}$$

In fact, the Kuramoto parameter represents the center of mass of the phases of the various neurons represented on the unitary circle, and therefore is a strong indication for their level of synchronization.

An insight into the nature of the bursty regime is provided by the Kuramoto parameter R and the global field $Y = \int_0^1 P(k_i) y_i(t) dk_i$ (already defined in Section 1.3.3) as a function of time. Figure 3.1 reveals that these quantities exhibit large temporal fluctuations.

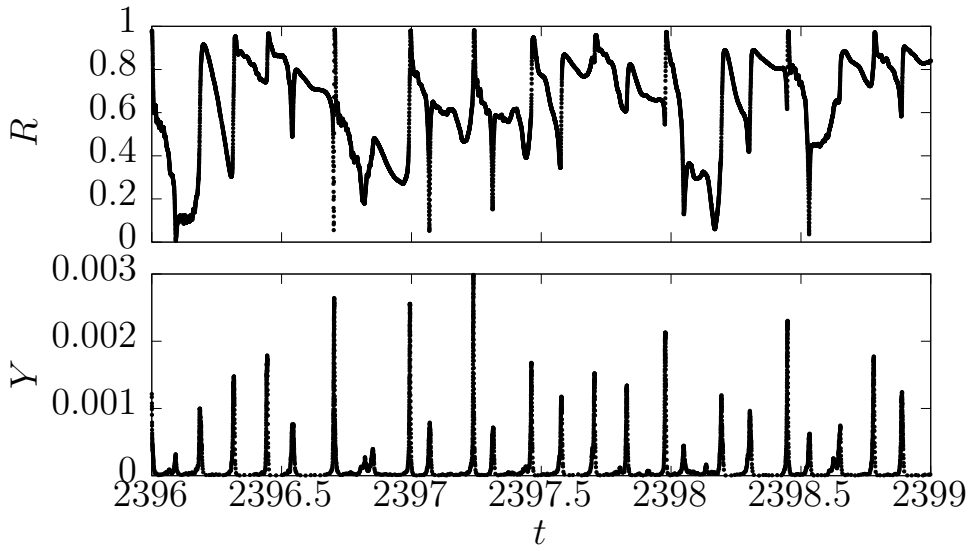

Figure 3.1. Kuramoto parameter $R(t)$ (upper panel) and synaptic global field $Y(t)$ (lower panel) as functions of time in the chaotic regime ($g = 10^5$, $\tau_{in} = 10^{-3}$, $N = 10^4$) in the DMF model.

In Figure 3.2 the time average R of the Kuramoto parameter and its fluctuations are displayed as a function of the coupling constant g.

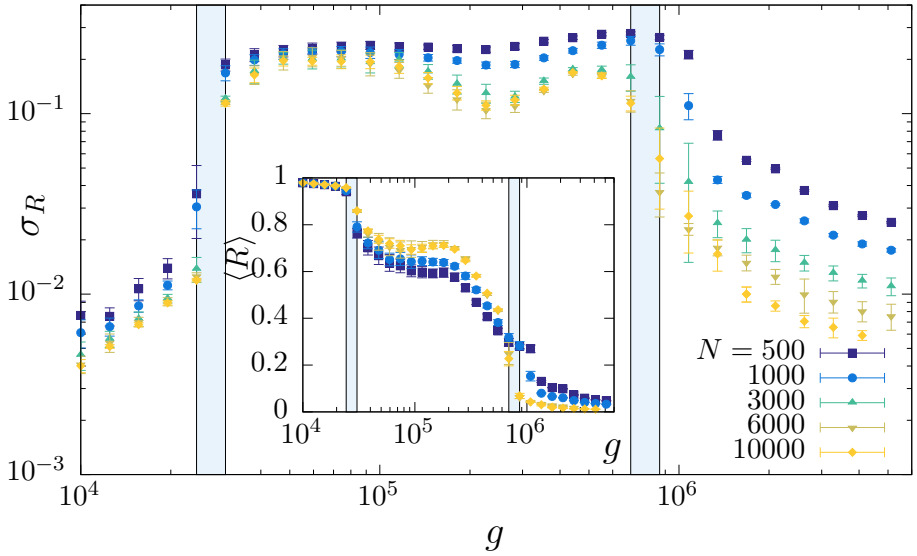

Figure 3.2. Standard deviation of the Kuramoto parameter, σ_R versus g for the DMF model with $\tau_{in} = 10^{-3}$ and five values of N. In the quasi-synchronous and bursty phases the data corresponding to the two larger values of N overlap within their statistical errors, indicating convergence in size, while deep in the asynchronous phase they decrease as $\sim N^{-1/2}$. Inset: temporal average of $R(t)$, showing that the larger sizes have attained their asymptotic value in all the three phases. The vertical stripes are common to all the figures in the article and indicate the apparent discontinuity of $\langle R \rangle$ for the largest sizes.

At small couplings,

$$\langle R \rangle \approx 1 \tag{3.7}$$

and the fluctuations are small, as the systems is in a *quasi-synchronous* phase. At large g, $\langle R \rangle$ becomes very small,

$$\langle R \rangle \to 0 \tag{3.8}$$

with increasing N, consistently with a periodic *asynchronous* phase. In the irregular, *bursty*, regime, $\langle R \rangle$ exhibits moderate values:

$$0 < \langle R \rangle < 1 \tag{3.9}$$

More significantly, its fluctuations grow abruptly by an order of magnitude; this is a signal of a complex dynamical phase, illustrated in Figure 3.1. The fluctuations of $\langle R \rangle$ originate from the alternations of synchronous events with asynchronous phases characterized by smaller bursts where only a subset of the neurons fires simultaneously.

3.1.1 Lyapunov exponents

The chaotic nature of the bursty dynamical regime is confirmed by the values of the Lyapunov exponents. Numerical evidence is provided by numerical simulations, showing that the largest Lyapunov exponent remains positive (only) in the bursty phase, even for the largest of the simulated sizes ($N = 2 \cdot 10^4$ for $\tau_{in} = 10^{-3}$), as shown in Figure 3.3 for a particular value of g.

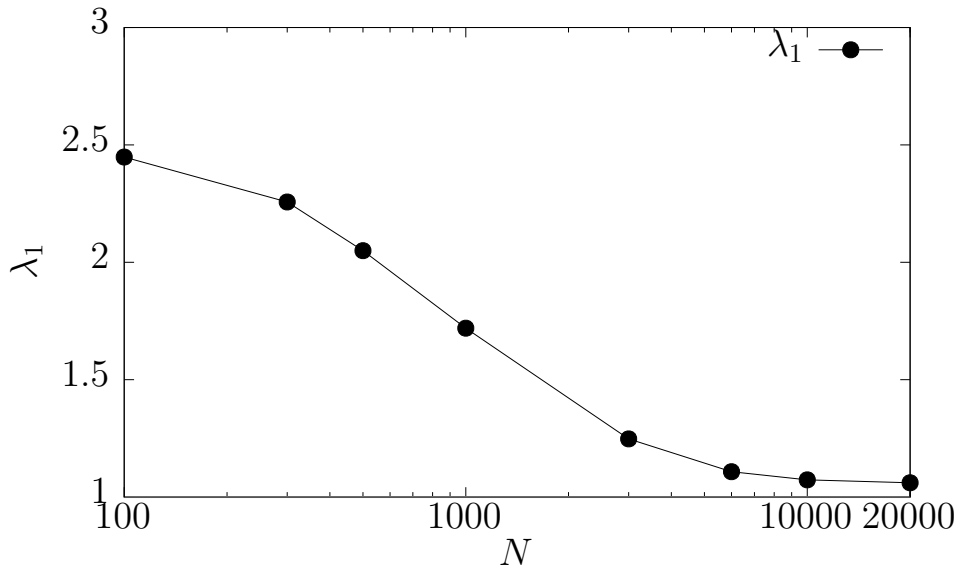

Figure 3.3. Finite-size scaling of the first Lyapunov exponent λ_1 as a function of the number N of sampled in-degrees in the DMF approach, with $\tau_{in} = 10^{-3}$ and $g = 3.10^4$.

3.1.2 Global Synaptic field

Figure 3.4 shows the global synaptic field received by the neurons $g\langle Y\rangle$. It is an increasing function of g. As we expect from our arguments in Section 2.1, the transition between quasi-periodic/bursty and bursty/asynchronous regimes occur when $g\langle Y\rangle$ is of the same order of magnitude of the leakage term

$$a - v(t) \sim O(1). \tag{3.10}$$

In particular, the value of $g\langle Y\rangle$ remains of order $a - v(t)$ (as shown in the first panel in Figure 3.4) even for large values of g (e.g. $g \sim 10^5$ in the bursty phase), since the resources are typically inactive during the evolution and $\langle Y\rangle$ assumes moderate values (notice that the amount of synaptic current received by the neurons in a centime time interval scales as $g\tau_{in}$). The second panel in Figure 3.4 shows that the fluctuations of $g\,\langle Y\rangle$,

$$g\,\langle \Delta_Y\rangle = g\sqrt{\langle Y^2\rangle - \langle Y\rangle^2} \tag{3.11}$$

are larger in the bursty regime.

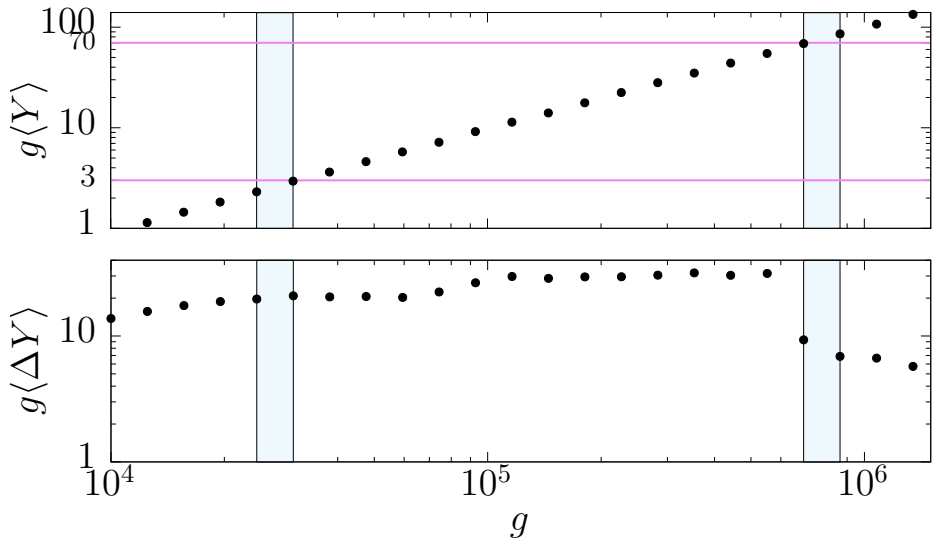

Figure 3.4. Higher panel: Average global synaptic field $\langle Y\rangle$ as a function of g in the Gaussian TUM model with $\tau_{in} = 10^{-3}$ and $N = 10^4$. The vertical stripes indicate the quasi-synchronous/bursty and bursty/asynchronous transitions. The horizontal line indicate the free neuron term $a - v$, revealing the value of g at which the bursty regime takes place. Lower panel: fluctuations of the synaptic field σ_Y multiplied by the coupling constant g.

3.1.3 Fluctuations of the interspike interval

Let us call $\Delta_i(t)$ the interspike interval corresponding to the last two events of the i-th degree, before the time t. The temporal average over the time index t, performed

as described in Subsection A.1, will be denoted by $\langle\cdot\rangle_t$, while the average over the i index will be denoted by

$$[\cdot]_i \equiv (1/N)\sum_{i=1}^{N}(\cdot). \tag{3.12}$$

In the MF case, the amount of temporal fluctuations of the unique interspike Δ_n around its average is called *coefficient of variation* (CV), and it is used as an order parameter discriminating among different regimes (see Figure 2.2). In the more complicated case of the disordered topology, two kinds of fluctuations of the interspike interval can be defined: those with respect to t, averaged over i, and those with respect to i, averaged over t:

$$\sigma_\Delta^2 = \langle [\Delta_i^2(t)]_i - [\Delta_i(t)]_i^2 \rangle_t \tag{3.13}$$

$$\sigma'^2_\Delta = \left[\langle \Delta_i^2(t) \rangle_t - \langle \Delta_i(t) \rangle_t^2 \right]_i \tag{3.14}$$

While the average interspike interval is

$$I = \langle [\Delta_i(t)]_i \rangle_t = [\langle \Delta_i(t) \rangle_t]_i. \tag{3.15}$$

We observe (see Figure 3.5) that for both definitions the fluctuations present a presumed discontinuity at g values compatible with the transition values (vertical stripes), at least for sufficiently large values of N, for which σ_Δ and σ'_Δ do no longer depend on N within their error-bars. While in the asynchronous and quasi-synchronous regimes $\sigma_\Delta/I < \sigma'_\Delta/I$, the situation is opposite in the bursty regime, where $\sigma_\Delta/I > \sigma'_\Delta/I$.

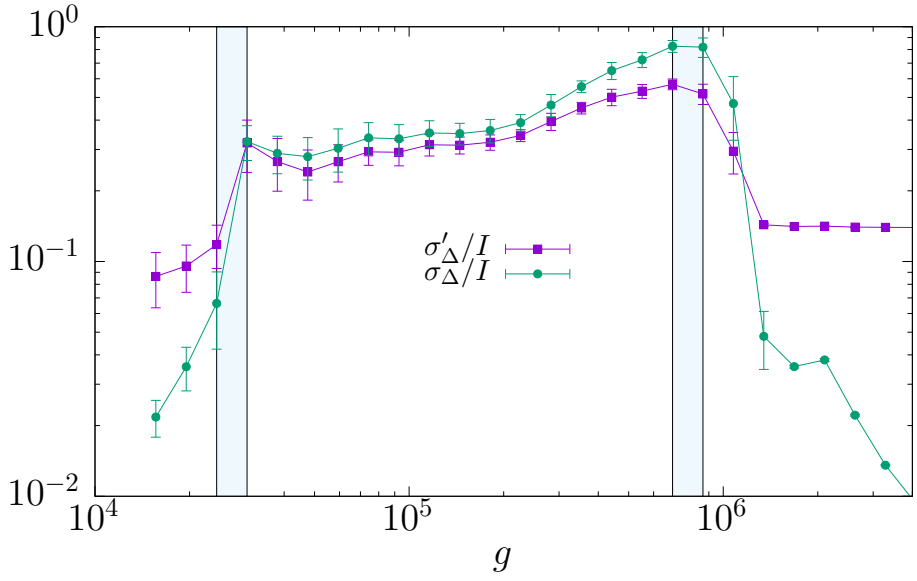

Figure 3.5. Two types of fluctuations of the interspike interval σ_Δ and σ'_Δ as a function of g, for the DMF model with $N = 500$, $\tau_{in} = 10^{-3}$. The apparent discontinuity of σ_Δ and σ'_Δ does not coincide with the bursty-asynchronous transition: this turns out to be, however, a finite-size effect absent for larger values of N.

3.2 Phase diagram

In this Section we address the natural issue of the relation between the chaotic phase in the single site MF model and the bursty-avalanche regime of the multi-site DMF approach. We have shown in Figure 3.3 that also the bursty phase is characterized by a chaotic dynamics with positive Lyapunov exponents. Moreover, in Figure 3.6 we have superimposed the dynamical phase diagrams of the MF and DMF models. In the DMF, the transitions points (circles) are set at the g intervals at which the abrupt increments of the fluctuations of the Kuramoto parameter take place (c.f. Fig. 3.2). In the MF case, the squares indicate the values of g at which the transitions to chaos occur.

While the phase diagrams slightly differ, the phase diagram of the DMF model converges continuously to that of the MF model in the limit of vanishing width of the distribution $P(k_i)$, as illustrated numerically in Section 3.2.1. This result clarifies the deep connection between the chaotic nature of the dynamics of Equations (2.3-2.5) and the emergence of the bursty regime.

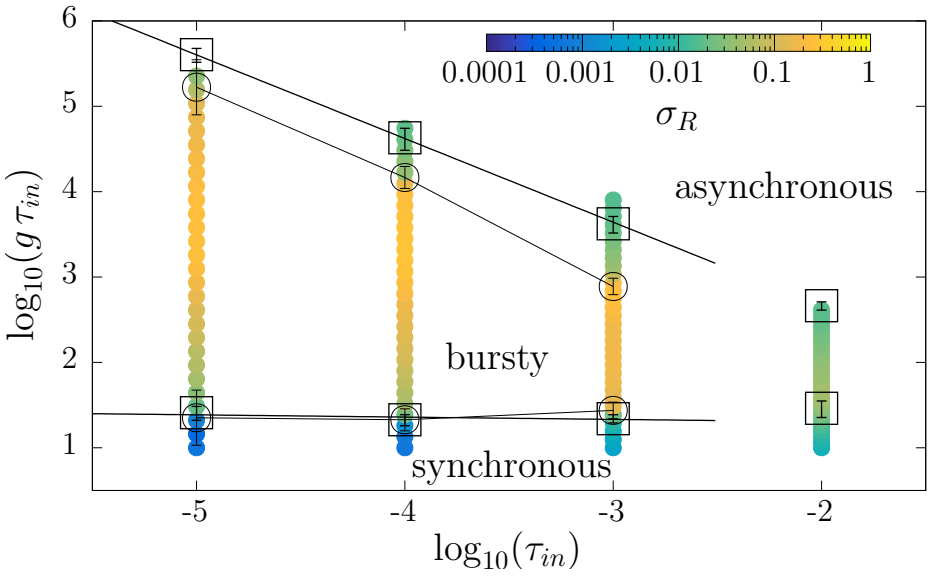

Figure 3.6. Dynamical phase diagram of the MF and DMF models in terms of the coupling constants g and of the synaptic time-scale $\tau_{\rm in}$. MF model: The squares indicate the g values at which the transition to chaos (along with the discontinuity of the interspike time standard deviation) takes place (see Section 2.2). The black lines are linear fits. DMF model: Each colored point corresponds to a simulation, the color code indicating σ_R at the corresponding value of $(g, \tau_{\rm in})$. The intervals of g containing the discontinuity (c.f. Fig. 3.2) are signaled with black circles.

The phase diagram in Figure 3.6 shows that the τ_{in}-dependence of the boundaries of the chaotic phase, g', g'' (squares), is consistent with the continuous lines, obtained by the weak and strong coupling limit arguments of section 2.1.

3.2.1 Comparison between the DMF and MF model phase diagrams

In the DMF model with a non-zero variance distribution $P(k)$, the two dynamical transitions occurring at $g = g_1$ and $g = g_2$, respectively between quasi-synchronous/bursty and bursty/asynchronous behaviors, do not coincide exactly with the two corresponding transitions to chaos g' and g'' in the pure MF model. However, in the limit of variance

$$\sigma \to 0, \tag{3.16}$$

we expect to recover the same transitions of the MF model, as it corresponds to a DMF with a delta function distribution $P(k)$ of the in-degrees. As a numerical confirmation, we have performed a series of simulations of the DMF model with Gaussian $P(k)$, with mean $\mu = 0.7$ and several decreasing values of σ. The results, in Figure 3.7, show indeed that the transition points g_1 and g_2 are compatible for small σ with the expected values (horizontal stripes) g' and g'' of the corresponding MF model. The transitions have been estimated by means of the discontinuity of the interspike interval fluctuations.

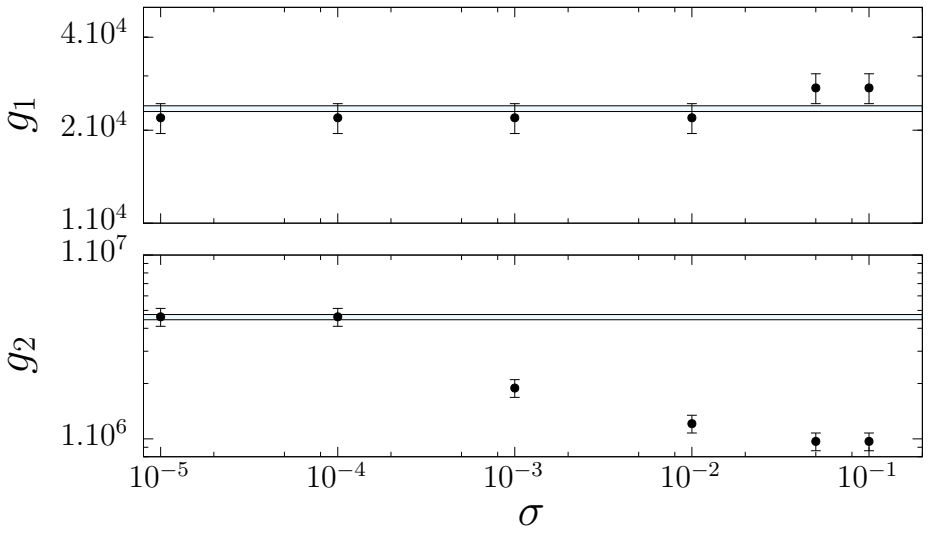

Figure 3.7. Transition interval of the synaptic couplings identifying the quasi-synchronous/bursty and bursty/asynchronous transitions (upper and lower panels, g_1 and g_2 respectively) for $\tau_{in} = 10^{-3}$, as a function of the variance σ of the Gaussian $P(k)$ distribution, whose average is $\mu = 0.7$. The horizontal stripes indicate the two respective values of the transition to chaos, g' and g'', in the MF model.

3.3 Power law distributed avalanches

In this Section we present the avalanche size distribution $h(s)$ of the DMF in the bursty regime. To compute $h(s)$, the *avalanche* is defined as a set of consecutive neuronal spikes such that all the interspike intervals of this set, $\{\Delta_n\}_n$, satisfy

$\Delta_n < \delta_t$, where δ_t is a threshold. The avalanche size distribution is consequently taken among various avalanche events during the temporal evolution. We have numerically checked that, for the cases of interest, there is a wide range of the threshold δ_t (of at least two orders of magnitude), for which the avalanche size distribution does not depend significantly on it (see Figure 3.9). The avalanche size distribution is consequently taken among various avalanche events during the temporal evolution [2].

The main plot of Figure 3.8 shows that the size s of the bursts, or avalanches, is broadly distributed. Interestingly, the distribution is compatible with a power law

$$h(s) \sim s^{-\gamma} \tag{3.17}$$

followed by a bump. The power γ, close to 2 (see Figure 3.10), does not depend significantly on N, nor on g for a wide g-range in the bursty phase. The peaks at large s in the distributions correspond to synchronous events where all neurons fire quasi-simultaneously, and their positions scale with the system size.

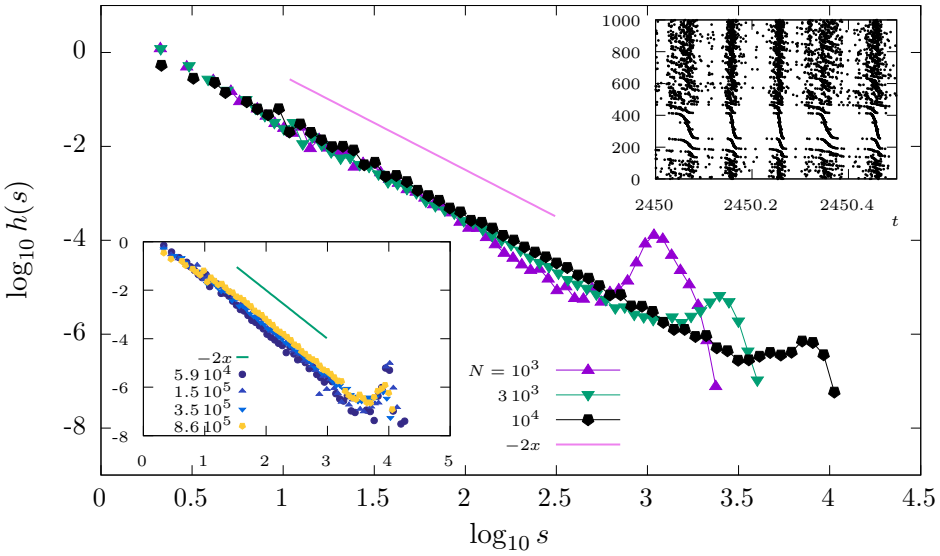

Figure 3.8. Avalanche size histogram $h(s)$ of the DMF model, $\tau_{in} = 10^{-3}$ and $g = 3.5 \cdot 10^5$ in the bursty regime, for several values of N. Upper inset: a fragment of the raster plot for the same system. Lower inset: $\log_{10} h(s)$ for $N = 10^4$ and various values of g across the bursty phase.

[2] Alternatively, the avalanche size can be simply defined as the number of neurons firing in a given time interval of width δ_w; one then constructs the histogram of the avalanche size over a sufficiently large number of such intervals, during the temporal evolution. We have numerically checked that both definitions of avalanche size distribution lead to analogous results.

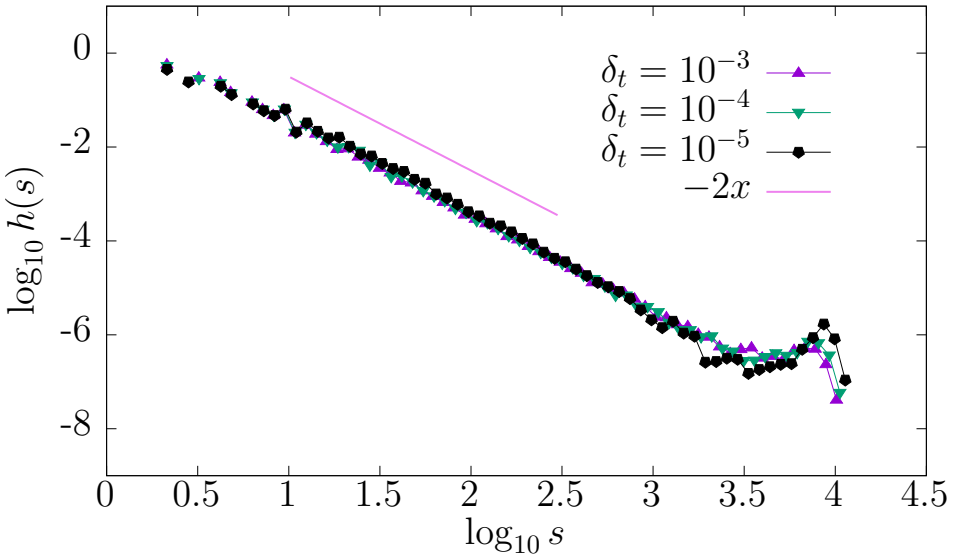

Figure 3.9. Avalanche size distribution of the DMF model with $\tau_{in} = 10^{-5}$, $N = 10^4$, $g = 10^7$, for three values of the threshold δ_t.

With this definition, the distribution of avalanche sizes, $h(s)$, becomes broadly distributed, as shown in Figure 3.8, and it is compatible with a power-law behavior for a wide range of values of g in the bursty phase ($[5.10^4 : 10^6]$, for $\tau_{in} = 10^{-3}$ and $N = 10^4$, 6.10^3), in a range of the size s of roughly three orders of magnitude (see Figure 3.10). The exponent γ, obtained by means of a linear fit in logarithmic scale, results to assume the values $\gamma_1 = -2.39 \pm 0.07$, $\gamma_2 = -2.07 \pm 0.04$ and $\gamma_3 = -2.08 \pm 0.05$, $\gamma_4 = -2.1 \pm 0.3$ for $g_1 \simeq 1.160 \cdot 10^5$, $g_2 \simeq 2.263 \cdot 10^5$, $g_3 \simeq 4.417 \cdot 10^5$, $g_4 = 1.07 \cdot 10^6$, respectively, for $N = 10^4$, and: $\gamma_1 = -2.42 \pm 0.25$, $\gamma_2 = -2.07 \pm 0.06$ and $\gamma_3 = -2.04 \pm 0.05$ for $N = 3 \cdot 10^3$ and the same values of the coupling constants g.

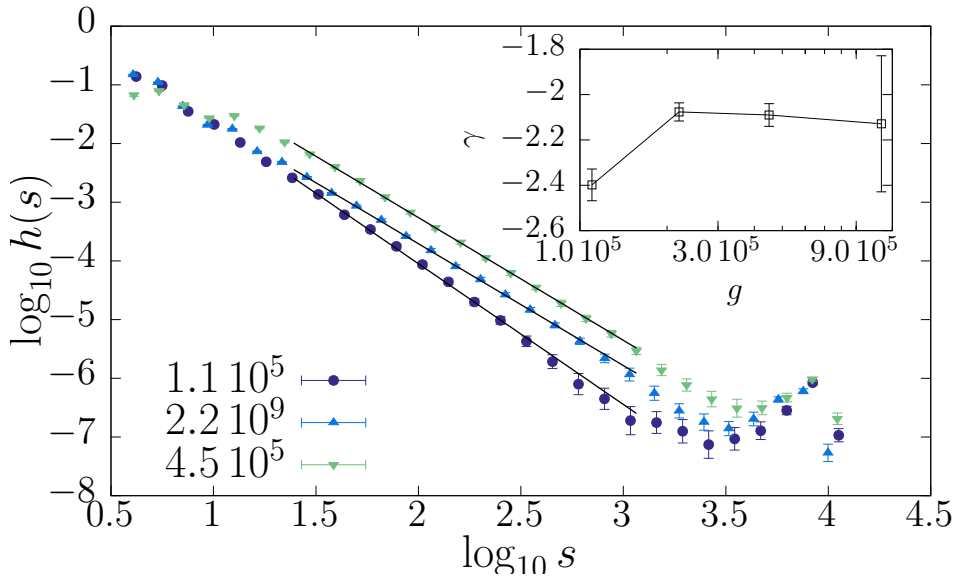

Figure 3.10. Avalanche size distribution for the system with $\tau_{in} = 10^{-3}$, $N = 10^4$ versus g. The straight lines are linear fits in an interval indicated by the x-axis range of the lines (the interval used for $g_4 \simeq 1.07 \cdot 10^6$ being $[2 : 3.5]$). The inset shows the value γ of the resulting slope versus g, for $N = 10^4$.

The error intervals are calculated as the interval of γ values for which the fit (performed in the intercept only) results to exhibit a value of the sum of squared residuals per degree of freedom lower than one. The fit takes into account the errors of the histogram points $h(s_i)$ (shown as error bars in the figure), which in their turn are calculated with a jackknife error estimation procedure: one blocks the data in blocks of sufficiently large size b, and estimates the the error of $h(s_i)$ as three times the standard deviation among the different histogram points in different blocks, $\{h_j(s_i)\}_j$.

Analogous results apply for the system with $\tau_{in} = 10^{-5}$, $N = 10^4$ in the g interval $[3.10^7, 5.10^{10}]$ in a range of the size s of three orders of magnitude.

3.4 Correlations and information

In the DMF model, the transition to the bursty collective behaviour also corresponds to the presence of large temporal correlations.

Another interesting quantity in temporal series of neural firing patterns is the amount of information they can sustain. In information theory, the Kolmogorov Complexity (KC) of a data sequence determines the length of the minimum computer program generating it, hence being a measure of the sequence predictability [43]. KC has been related to the computational power of artificial neural networks [5], and used in the quantitative characterization of epileptic EEG recordings [58].

3.4.1 Temporal correlations

We define the time-dependent *complex correlation* of the N-neuron system:

$$c_N(\delta, t) = \frac{1}{N} \sum_{n=1}^{N} e^{\imath\phi_i(t)} e^{-\imath\phi_i(t+\delta)}, \tag{3.18}$$

where $\phi_i(t)$ is the Kuramoto phase (3.5) of neuron i at time t and $\imath$ is the imaginary unit, along with the *connected correlation function*:

$$C_N(\delta) = |\langle c_N(\delta, t)\rangle_t| - |\langle c_N(\mathcal{T}, t)\rangle_t|. \tag{3.19}$$

The connected correlation, C, is obtained from the complex correlation as the temporal average $\langle\cdot\rangle_t$ of c over a sufficiently large interval of times t and by subtracting its asymptotic stationary value $|\langle c_N(\mathcal{T}, t)\rangle_t|$ at a sufficiently large value of the time difference, $\delta = \mathcal{T}$, such that c_N does no longer significantly (beyond its fluctuations) depend on $\mathcal{T}$.

The average over the time variable t is a temporal average over M instants of time equispaced by a time interval τ, i.e.:

$$\langle\cdot\rangle_t = M^{-1} \sum_{m=1}^{M} \cdot\, \delta(t,\, m\tau + t_0), \tag{3.20}$$

where t_0 is a reference initial time and δ is the Kronecker delta. To perform the average, we have chosen a small τ, much lower than the average interspike interval at the corresponding value of the parameters (g, τ_{in}), and a sufficiently large M so that the resulting $|\langle c_N(\delta, t)\rangle_t|$ results unchanged for larger values of M and for lower values of τ, given N and a range of δ.

$C(\delta)$ measures in this way the average amount of correlation between spike configurations separated by a time delay δ.

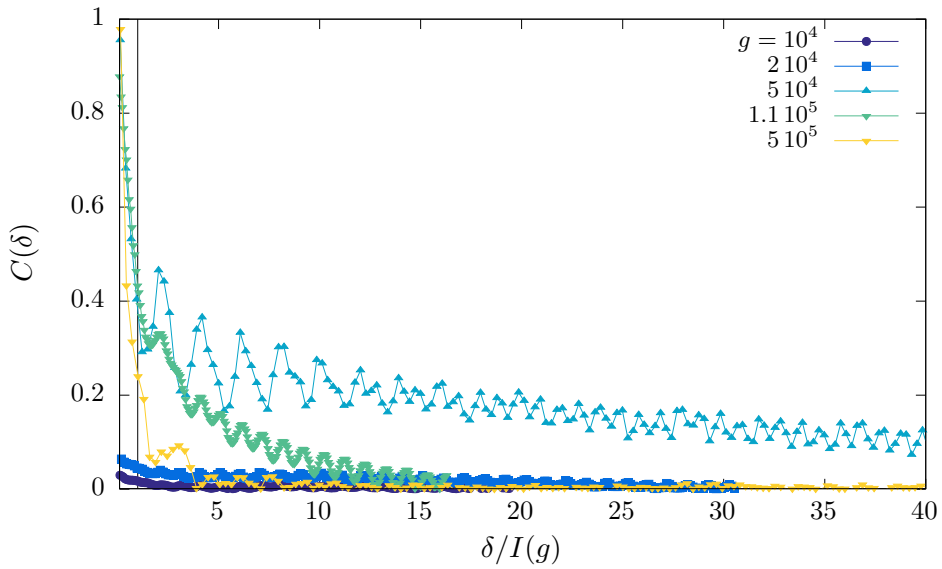

Figure 3.11. Connected correlation function C as a function of the time difference δ in units of the average interspike time $I(g)$, for several values of g in the DMF model with $\tau_{in} = 10^{-3}$, $N = 800$. For values of g in the bursty phase, the correlation remains high even after large time differences.

The quantity $C(\delta)$ (see Fig. 3.11) reveals the existence of large correlations for times δ much larger than the average interspike time, $I(g)$, only in the bursty regime (for $3 \cdot 10^4 \lesssim g \lesssim 10^5$ at $\tau_{in} = 10^{-3}$), while in the synchronous and asynchronous regimes, $C(\delta)$ decays faster to its asymptotic value.

It is worth mentioning a delicate aspect in the numerical estimation of the asymptotic value of the correlation. In the asynchronous regime, the (disconnected) complex correlation $c_N(\delta, t)$ decreases very fast for moderate values of δ, of the order of the average interspike interval that the determination of the asymptotic correlation is unambiguous. In the quasi-synchronous regime, we expect c_N to achieve a non-zero value for arbitrarily large values of δ - at least in the large-N limit. A set $\mathcal{S}$ of synchronous neurons with a constant period is present in this limit, so that their Kuramoto phase delays $\phi_i(t) - \phi_i(t+\delta)$ are constant for all δ and $i \in \mathcal{S}$. Equation (3.18) remains therefore finite for any δ) [22].

For finite values of N, however, the period of synchronized neurons is not exactly constant in time nor in the neuron index (a fact that has been related with the weak chaos exhibited by the model [22, 13]). This reflects in the fact that, in the quasi-synchronous regime, $|c_N(\delta, t)|$ rapidly decays as a function of δ. As expected, it starts to oscillate around a nonzero value which begins to slowly decrease for larger values of δ (the slower the larger the value of N). For large N and moderate δ, this phenomenon is not observed in our numerical calculations, but it becomes an issue in the numerical estimation of the asymptotic value at a very large time delays, $\mathcal{T}$. To construct the upper panel of Figure 5 of the main article, we have estimated the average value of $|c_N(\mathcal{T}, t)|$, $\mathcal{T}$ being twice the maximum value of δ used in the figure abscissa, for which the asymptotic value still does not change significantly by doubling N or M (although, we warn, this value is not the stationary value for

arbitrarily large values of $\mathcal{T}$ or M). In other words, to compute the quantity $C_N(t)$ in the quasi-synchronous regime, we have assumed that the quantity c_N stays constant in δ for infinite N (an hypothesis with which our numerical data is compatible). A similar (but less significant for the final shape of C_N) strong finite-size effect is found in the bursty regime for large values of δ. In any case, the asymptotic value reached by $|c_N(\delta, t)|$ for moderate values of δ, changes abruptly with g: in the synchronous regime it is close, but not equal, to the squared Kuramoto parameter; for g in the bursty regime, it decreases towards a number smaller than the oscillation amplitude.

Alternative ways of defining temporal correlations

We end this section proposing an alternative definition of temporal correlation function:

$$C'_N(\delta) = |\langle K_N(t)\, K_N(t+\delta)^* \rangle_t|, \tag{3.21}$$

where

$$K_N = \frac{1}{N} \sum_{i=1}^{N} \exp(\imath \phi_i(t)) \tag{3.22}$$

is the (complex) Kuramoto parameter. The qualitative behavior of both definitions is quite similar (they differ in the fact that the first definition, Equation (3.19), accounts for the correlations between neurons with equal coupling k_i only), although the finite-size behavior of the latter definition results to be slower in our numerical analysis. We have consequently used the first definition to draw our conclusions about the system temporal correlations.

3.4.2 Kolmogorov Complexity

We consider the KC of the model raster plot, interpreting it as an estimation of the amount of information that can be codified in the dynamical signal. The numerical results for the DMF model reveal that the KC as a function of g (see Fig. 3.12) presents a maximum within the bursty regime (around $g \simeq 6\,10^4$ for $\tau_{in} = 10^{-3}$).

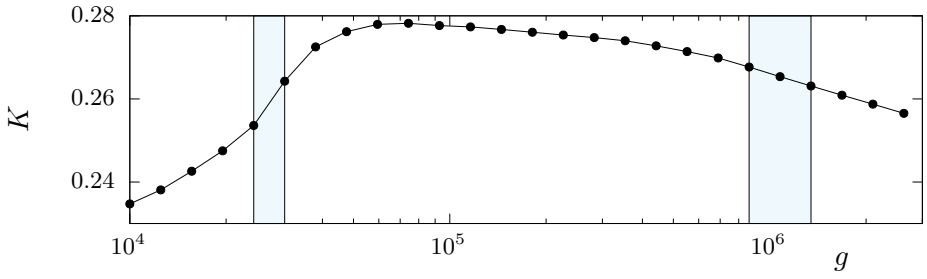

Figure 3.12. Kolmogorov Complexity of the DMF model, $\tau_{in} = 10^{-3}$, $N = 10^3$, and the spike time differences Δ_n stored with 14 digits of precision.

We have considered the Kolmogorov complexity (KC) of the raster plot of the Gaussian model, for several values of g across three model regimes. In particular,

we consider the sequence of differences of spike times Δ_n (not writing the spiking neuron index), and estimate [36] the KC of such sequences as the size of the zipped file containing the sequence, divided by the size of the original file. In practical terms, we use the *gzip* algorithm to compress the file containing a sequence of L spiking times (written in ascii with constant number of digits), corresponding to a simulation of the TUM model with a given set of parameters $\{\sigma\}$. We then compute K_L as the ratio of the compressed file size over the original file size. We avoid writing in the original file data corresponding to the transient, by skipping a large enough amount of initial events. In this circumstance, we observe that, for large enough number of events (i.e., of lines in the original file) L,

$$K_L \simeq K \tag{3.23}$$

does not depend significantly on L, we take then K as the estimation of the KC of $\{\sigma\}$. The number of digits n used to store the spiking times being large enough, has the mere influence of shifting the whole K versus $\{\sigma\}$ curve by an n-depending constant.

In the presence of a quasi-synchronous to asynchronous regime transition, the KC presents a maximum at the parameters $\{\sigma\}$ corresponding to the transition value. In the presence of the bursty regime presented and characterized in this work, one observes that the bursty regime presents a higher value of the KC, the maximum of which is found for values of g in the bulk bursty regime, i.e. larger than the quasi-synchronous/asynchronous transition value.

))))))))))

Conclusions

In this thesis we have reported the existence of a new dynamical phase occurring in a network of purely excitatory LIF neurons connected with synaptic plasticity. This phase is strongly chaotic and differs from previously known irregular phases for similar models, e.g. phases with chaotic transient dynamics [17, 75]. The chaotic phase must also be distinguished from previous irregular regimes observed in spiking neural models, namely *weak chaos* in purely excitatory disordered networks [53] or *stable chaos* in inhibitory ones [74, 68, 56].

The collective chaotic phase is preserved in the network of purely excitatory leaky integrate-and-fire neurons with short term synaptic plasticity in presence of disordered couplings, both in the disordered version of the mean field and in the version of the network in which its metric structure is taken into account. In that case, interestingly, the chaotic phase also features characteristic power law scaling of activity events (in particular in the distribution of *avalanches*).

The main result of the thesis is then to propose a dynamical mechanism, based on neurophysiological modelling for short term synaptic plasticity, that reproduces the observed avalanches phases and contains the key elements able to dynamically generate this complex regime. Our analysis reveals a general framework for the generation of irregular avalanches that emerges from the combination of disorder and deterministic underlying chaotic dynamics. More specifically, we have emphasized an unknown connection between synchronous chaos and disorder in the connectivities and in the coupling constants, that together cooperate to produce the mechanism that we suggest to be at the basis of the avalanche regime.

The dynamical phase diagram that we have been able to compute exhibits two dynamical transitions from quasi-synchronous and asynchronous regimes [23] to the nontrivial, collective, bursty regime with avalanches. The emergent complex regime occurs in a large region of the phase diagram. In the homogeneous case without disorder, the system synchronizes and the bursty behavior is reflected into a period doubling transition to chaos for a two dimensional discrete map. Numerical simulations show that the bursty chaotic phase with avalanches exhibits a spontaneous emergence of time correlations and enhanced Kolmogorov complexity.

By properly defining temporal correlations and by using tools from information theory, we show that this additional phase is strongly correlated and it carries a relevant amount of information compared to the previously known, and less complex, dynamical phases.

Through the comparison of the deactivation time scale τ_{in} with the experimental timescales, we have suggested a potential relationship between the time scale of decay of the receptor and the intrinsic period of the neuron (two measurable quantities) as

a guide for the emergence of a complex bursty regime.

Finally, our analysis uncovers a general mechanism relating stability properties and emergent avalanche activity in the presence of short-term synaptic plasticity, that may go beyond our particular case of study and could be active also in different frameworks featuring the same dynamical ingredients.

Appendix

Appendix A

Simulation protocol and measures

In this section we discuss in more detail the numerical analysis of the MF and DMF models. As said in the results part of this thesis, the DMF model consists in N nodes representing neurons with in-degree Nk_i extracted from a probability distribution $P(k_i)$. When not specified differently, the numerical results correspond to simulations performed with a Gaussian probability distribution $P(k)$, with mean $\mu = 0.7$ and variance $\sigma = 0.077$.

A.1 Event-driven dynamics simulation protocol

We have simulated finite-size realizations of the event-driven dynamics, Equations (3.1) with number of neurons N. The temporal averages and second moments of the relevant observables (Kuramoto parameter and neuron-averaged interspike interval) are, in principle, a time integral. We have approximated it by a sum evaluated in equispaced times separated by an interval, much shorter than the average interspike interval, over sufficiently large temporal windows. We have discarded the initial *transient* regime, whose length is strongly dependent on the initial condition and on the values of g, τ_{in}. To shorten the length of the transient in series of simulations at different but close values of g, we take as an initial condition for the dynamic variables of a simulation at a given g, the final configuration attained by the simulation at the immediately lower value g. We have also checked the opposite protocol, reducing the value of g and taking as initial condition the final configuration of the precedent simulation, verifying that both protocols lead to identical results.

The stationarity of the average and standard deviation of the Kuramoto parameter and of the interspike interval has been verified comparing the results obtained averaging over temporal windows of exponentially larger and larger width. Moreover, the width W of the temporal window is considered to be large enough if the averages of the considered observable over sub-windows of the interval (of size $b \ll W$) result statistically uncorrelated (i.e., if not only their average but their fluctuations over different sub-windows do no longer grow significantly with increasing b). With this method (the jackknife method), we ensure that W is much larger than the correlation time of the considered observable.

Appendix B

Robustness of the results

B.1 Robustness with respect to the shape of the distribution $P(k_i)$.

A natural question concerns the robustness of the results with respect to the shape of the coupling distribution. In Figure B.1 we plot the avalanche size distribution and the raster plot for couplings extracted from a Gamma function distribution i.e.

$$P(k_i) = \gamma_{m,\theta}(k) = \frac{1}{\theta^m \Gamma(m)} k_i^{m-1} e^{-\frac{k_i}{\theta}}, \tag{B.1}$$

where $\Gamma(n)$ is the Euler Gamma-function. Figure B.1 shows that the bursty regime is observed also in this case, in the presence of an asymmetric distribution.

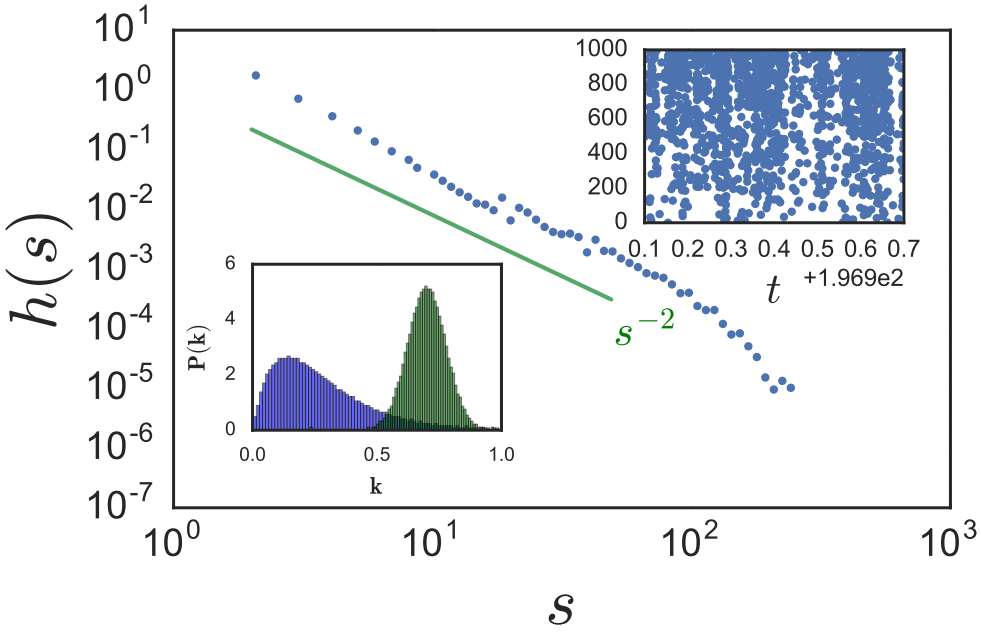

Figure B.1. Numerical results for a coupling distribution $P(k_i)$ being a Gamma function defined by equation (B.1) with $m = 2$ and $\theta = 0.14$. The parameter of the simulations are $a = 1.3$, $g = 10^5$, $\tau_{in} = 10^{-3}$, $\tau_R = 10$ and the number of neurons is $N = 1000$. The main plot represents the distribution h of the avalanches sizes s, while the upper inset is the raster plot and the lower inset is a comparison between the Gamma distribution (in blue) and the Gaussian distribution with $\mu = 0.7$ and $\sigma = 0.077$ (in green).

B.2 Robustness with respect to the single neuron time scale.

The phase diagram we obtained has been described in terms of the coupling constant g and of the synaptic timescales τ_{in} and τ_R. However, the system is characterized by another natural timescale, i.e. the oscillation period

$$T = \log\left(\frac{a}{a-1}\right) \tag{B.2}$$

of an isolated neuron. In our simulations $a = 1.3$ so that $T \approx 1$. Furthermore, another time scale is present in the system, the membrane time constant τ_m that rescales all time scales of the model. In practice, in order to obtain the physical value of a time scale, we need to multiply such value for τ_m, and in physical system $\tau_m \approx 20 - 80$ ms.

Letting $a \to 1$ one obtains a much slower dynamics for the isolated neuron. Physically, a change in a corresponds to a variation of the leakage current, which does not correspond to a trivial redefinition of the timescales since the parameter a drives the non linearity of the evolution, that is the time of the resetting to zero of the potential v_i. In figure B.2 we show the raster plot and the avalanches size distribution for a system with $a = 1.0001$ ($T \approx 9.2$, i.e. if $\tau_m = 30$ ms we consider a

neuron firing intrinsically at 3.5 Hz). In this case the bursty regime is recovered for $\tau_{in} = 0.1$, so it is not necessary that $\tau_{in} \ll 1$. We remark that experimental data analysis about receptors in the cortex suggest that the inactivation time is around 3 ms (i.e. $\tau_{in} = 0.1$ if $\tau_m = 30$ ms) [65, 66].

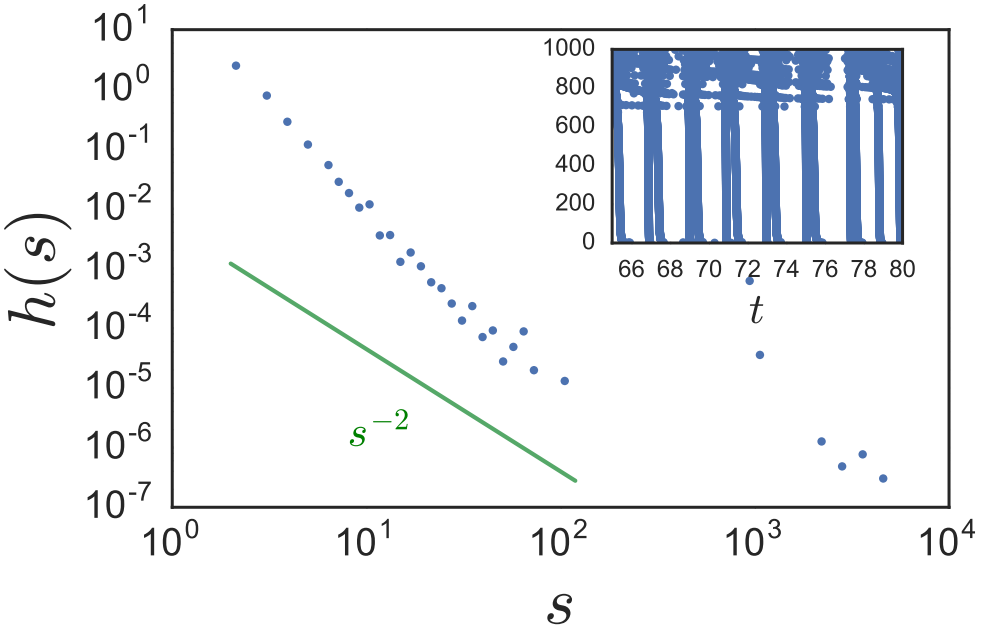

Figure B.2. Numerical results for a system with $a = 1.0001$, $g = 120$, $\tau_{in} = 10^{-1}$, $\tau_R = 10$, $N = 1000$. The coupling distribution $P(k_i)$ is a Gaussian with average $\mu = 0.7$ and variance $\sigma = 0.077$. The main plot represents the distribution h of the avalanches sizes s, while the inset is the raster plot.

B.3 Degree based mean field and finite connectivity systems.

In [13, 22] it has been shown that the DMF approach can be used to study also systems with large but finite connectivities; i.e. neural networks where the interactions are described by a directed adjacency matrix ϵ_{ij} with a large enough number of incoming synapse $k_i^{in} = \sum_j \epsilon_{ij}$. In this case the first of Equations (1.31-1.33) reads:

$$\dot{v}_i(t) = a - v_i(t) + \frac{g}{N} \sum_{j \neq i}^{N} \epsilon_{i,j} y_j(t) \tag{B.3}$$

while the last two remain unchanged. However, in [13, 22], only the synchronous and the asynchronous regimes have been observated.

In Figure B.3 we show the raster plot and the avalanches size distribution in a finite connectivity neural network in the bursty regime. In particular, we focus on a random network where for each node the incoming degree is chosen from a distribution

$$P'(k_i^{in}) = \mathcal{N}(N\mu, N\sigma) \tag{B.4}$$

(where $\mathcal{N}(x, y)$ is the Gaussian distribution with mean x and standard deviation y) and we set the parameters to a value where the DMF model exhibits burstyness. Simulations show that also in a finite connectivity networks, where a metric can be introduced, the dynamics is bursty and the avalanche distribution is characterized by a power law whose exponent is approximatively -2.

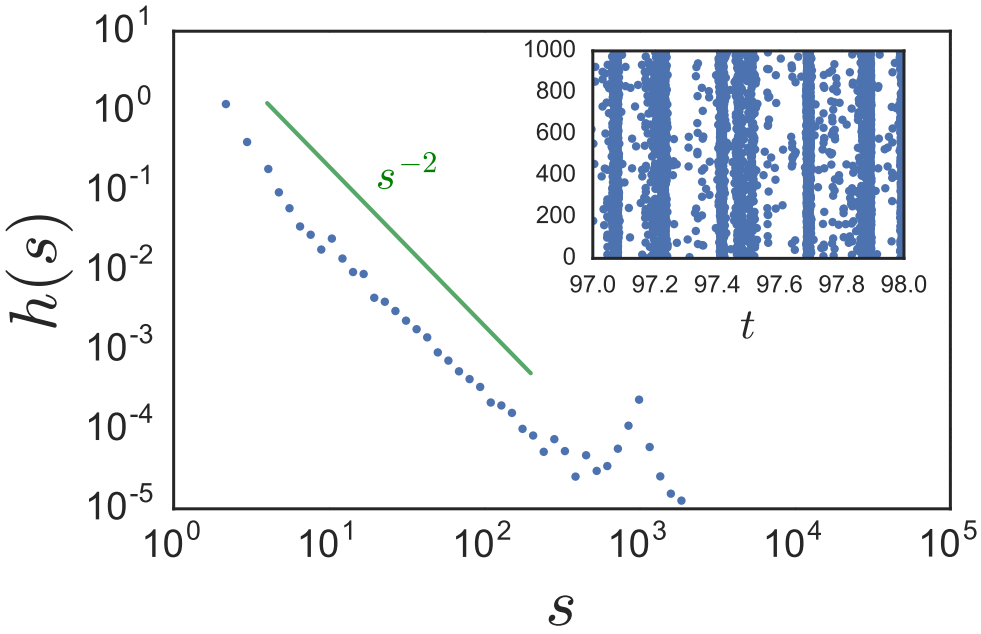

Figure B.3. Numerical results for a random finite connectivity network whit $a = 1.3$, $g = 10^5$, $\tau_{in} = 10^{-3}$, $\tau_R = 10$, $N = 1000$. The incoming degree distribution $P'(k_i^{in})$ is a Gaussian with average $\mu = 0.7N$ and variance $\sigma = 0.077N$. The main plot represents the distribution h of the avalanches sizes s, while the inset is the raster plot.

Bibliography

[1] Abbott, L. F. and van Vreeswijk, C. Asynchronous states in networks of pulse-coupled oscillators. *Phys. Rev. E*, **48** (1993), 1483. Available from: http://link.aps.org/doi/10.1103/PhysRevE.48.1483.

[2] Abeles, M. *Corticonics*. New York: Cambridge UP (1991).

[3] Acebrón, J. A., Bonilla, L. L., Pérez Vicente, C. J., Ritort, F., and Spigler, R. The kuramoto model: A simple paradigm for synchronization phenomena. *Rev. Mod. Phys.*, **77** (2005), 137. Available from: http://link.aps.org/doi/10.1103/RevModPhys.77.137.

[4] Amit, D. J. and Brunel, N. Model of global spontaneous activity and local structured activity during delay periods in the cerebral cortex. *Cereb. Cortex*, **7** (1997), 237. Available from: http://cercor.oxfordjournals.org/content/7/3/237.abstract.

[5] Balcazar, J. L., Gavalda, R., and Siegelmann, H. T. Computational power of neural networks: a characterization in terms of kolmogorov complexity. *IEEE Trans. Inf. Theory*, **43** (1997), 1175. doi:10.1109/18.605580.

[6] Barrat, A., Barthelemy, M., and Vespignani, A. *Dynamical Processes on Complex Networks*. Cambridge University Press (2008).

[7] Beggs, J. M. and Plenz, D. Neuronal avalanches in neocortical circuits. *J. Neurosci.*, **23** (2003), 11167. Available from: http://www.jneurosci.org/content/23/35/11167.abstract.

[8] Benettin, G., Galgani, L., Giorgilli, A., and Strelcyn, J.-M. Lyapunov characteristic exponents for smooth dynamical systems and for hamiltonian systems; a method for computing all of them. part 1: Theory. *Meccanica*, **15** (1980), 9. Available from: http://dx.doi.org/10.1007/BF02128236.

[9] Bonachela, J. A., de Franciscis, S., Torres, J. J., and Muñoz, M. A. Self-organization without conservation: are neuronal avalanches generically critical? *J. Stat. Mech. P02015*, (2010). Available from: http://stacks.iop.org/1742-5468/2010/i=02/a=P02015.

[10] Bonachela, J. A. and Muñoz, M. A. Self-organization without conservation: true or just apparent scale-invariance? *J. Stat. Mech. P09009*, (2009). Available from: http://stacks.iop.org/1742-5468/2009/i=09/a=P09009.

[11] Brette, R. Exact Simulation of Integrate-and-Fire Models with Exponential Currents. *Neural Comput.*, **19** (2007), 2604. Available from: http://dx.doi.org/10.1162/neco.2007.19.10.2604, doi:10.1162/neco.2007.19.10.2604.

[12] Brunel, N. Dynamics of sparsely connected networks of excitatory and inhibitory spiking neurons. *J. Comput. Neurosci.*, **8** (2000), 183. Available from: http://dx.doi.org/10.1023/A:1008925309027.

[13] Burioni, R., Casartelli, M., di Volo, M., Livi, R., and Vezzani, A. Average synaptic activity and neural networks topology: a global inverse problem. *Sci. Rep.*, **4** (2014), 4336. Available from: http://www.nature.com/articles/srep04336.

[14] Burns, B. D. and Webb, A. C. The spontaneous activity of neurones in the cat's cerebral cortex. *Proc. R. Soc. B*, **194** (1976), 211. Available from: http://rspb.royalsocietypublishing.org/content/194/1115/211, doi:10.1098/rspb.1976.0074.

[15] Chialvo, D. R. Emergent complex neural dynamics. *Nat. Phys.*, **6** (2010), 744. Available from: http://dx.doi.org/10.1038/nphys1803.

[16] Chung, F. and Lu, L. *Complex Graphs and Networks*. CBMS Series in Mathematics, AMS (2004).

[17] Cortes, J. M., Desroches, M., Rodrigues, S., Veltz, R., Muñoz, M. A., and Sejnowski, T. J. Short-term synaptic plasticity in the deterministic tsodyks–markram model leads to unpredictable network dynamics. *Proc. Natl. Acad. Sci. U.S.A.*, **110** (2013), 16610. Available from: http://www.pnas.org/content/110/41/16610.short.

[18] de Arcangelis, L., Perrone-Capano, C., and Herrmann, H. J. Self-organized criticality model for brain plasticity. *Phys. Rev. Lett.*, **96** (2006), 028107. Available from: http://link.aps.org/doi/10.1103/PhysRevLett.96.028107.

[19] Destexhe, A., Hughes, S. W., Rudolph, M., and Crunelli, V. Are corticothalamic ?up?states fragments of wakefulness? *Trends Neurosci.*, **30** (2007), 334. Available from: http://www.cell.com/trends/neurosciences/abstract/S0166-2236(07)00100-2?_returnURL=http%3A%2F%2Flinkinghub.elsevier.com%2Fretrieve%2Fpii%2FS0166223607001002%3Fshowall%3Dtrue.

[20] di Santo, S., Burioni, R., Vezzani, A., and Muñoz, M. A. Self-organized bistability associated with first-order phase transitions. *Phys. Rev. Lett.*, **116** (2016), 240601. Available from: http://journals.aps.org/prl/abstract/10.1103/PhysRevLett.116.240601.

[21] di Volo, M. *Dynamics, synchronization and inverse problem in mean field neural networks with synaptic plasticity*. PhD Thesis, Parma University (2014).

[22] di Volo, M., Burioni, R., Casartelli, M., Livi, R., and Vezzani, A. Heterogeneous mean field for neural networks with short-term plasticity. *Phys. Rev. E*, **90** (2014), 022811. Available from: http://link.aps.org/doi/10.1103/PhysRevE.90.022811.

[23] di Volo, M., Livi, R., Luccioli, S., Politi, A., and Torcini, A. Synchronous dynamics in the presence of short-term plasticity. *Phys. Rev. E*, **87** (2013), 032801. Available from: http://link.aps.org/doi/10.1103/PhysRevE.87.032801.

[24] Ding, M. and Yang, W. Stability of synchronous chaos and on-off intermittency in coupled map lattices. *Phys. Rev. E*, **56** (1997), 4009. Available from: http://link.aps.org/doi/10.1103/PhysRevE.56.4009.

[25] El Boustani, S., Marre, O., Béhuret, S., Baudot, P., Yger, P., Bal, T., Destexhe, A., and Frégnac, Y. Network-state modulation of power-law frequency-scaling in visual cortical neurons. *PLoS Comput. Biol.*, **5** (2009), e1000519. Available from: http://journals.plos.org/ploscompbiol/article?id=10.1371/journal.pcbi.1000519.

[26] Elias, L. J. and Saucier, D. M. *Neuropsychology: Clinical and Experimental Foundations*. Boston: Pearson (2005).

[27] Gerstner, W., Kistler, W. M., Naud, R., and Paninski, L. *Neuronal Dynamics*. Cambridge University Press (2014).

[28] Goncalves, J. T., Anstey, J. E., Golshani, P., and Portera-Cailliau, C. Circuit level defects in the developing neocortex of fragile x mice. *Phys. Rev. E*, **56** (2013), 903. Available from: http://dx.doi.org/10.1038/nn.3415.

[29] Haas, L. F. Hans berger (1873–1941), richard caton (1842–1926), and electroencephalography. *J. Neurol. Neurosurg. Psychiatry*, **74** (2003), 9.

[30] Hansel, D. and Mato, G. Asynchronous states and the emergence of synchrony in large networks of interacting excitatory and inhibitory neurons. *Neural Comput.*, **15** (2003), 1. Available from: http://www.mitpressjournals.org/doi/abs/10.1162/089976603321043685?url_ver=Z39.88-2003&rfr_id=ori:rid:crossref.org&rfr_dat=cr_pub%3dpubmed#.V9xEyJNS2QM.

[31] Heagy, J. F., Carroll, T. L., and Pecora, L. M. Synchronous chaos in coupled oscillator systems. *Phys. Rev. E*, **50** (1994), 1874. Available from: http://link.aps.org/doi/10.1103/PhysRevE.50.1874.

[32] Hesse, J. and Gross, T. Self-organized criticality as a fundamental property of neural systems. *Front. Syst. Neurosci.*, **8** (2014). Available from: http://www.frontiersin.org/systems_neuroscience/10.3389/fnsys.2014.00166/abstract.

[33] Hulata, E., Volman, V., and Ben-Jacob, E. Self-regulated complexity in neural networks. *Nat. Comput.*, **4** (2005), 363. Available from: http://link.springer.com/article/10.1007/s11047-005-3668-5.

[34] Izhikevich, E. M. Which model to use for cortical spiking neurons? *IEEE Trans. Neural Networ.*, **15** (2004), 1063. doi:10.1109/TNN.2004.832719.

[35] Kadmon, J. and Sompolinsky, H. Transition to chaos in random neuronal networks. *Phys. Rev. X*, **5** (2015), 041030. Available from: http://link.aps.org/doi/10.1103/PhysRevX.5.041030.

[36] Kaitchenko, A. Algorithms for estimating information distance with application to bioinformatics and linguistics. In *Canadian Conference on Electrical and Computer Engineering, 2004*, vol. 4, p. 2255 (2004). Available from: http://ieeexplore.ieee.org/document/1347695/.

[37] Kandel, E., Schwartz, J., Jessell, T., Siegelbaum, S. A., and Hudspeth, A. J. *Principles of Neural Science (5th ed.)*. McGraw-Hill (2013).

[38] Kinouchi, O. and Copelli, M. Optimal dynamic range of excitable networks at criticality. *Nat. Phys.*, **2** (2006), 348. Available from: http://www.escet.urjc.es/~fisica/msanjuan/complejidad/natphys_psychophys06.pdf.

[39] Kirst, C., Geisel, T., and Timme, M. Sequential desynchronization in networks of spiking neurons with partial reset. *Phys. Rev. Lett.*, **102** (2009), 068101. Available from: http://link.aps.org/doi/10.1103/PhysRevLett.102.068101.

[40] Lapicque, L. Quantitative investigations of electrical nerve excitation treated as polarization. *J. Physiol. Pathol. Gen.*, **9** (1907), 620.

[41] Levina, A., Herrmann, J. M., and Geisel, T. Dynamical synapses causing self-organized criticality in neural networks. *Nat. Phys.*, **3** (2007), 857. Available from: http://www.nature.com/doifinder/10.1038/nphys758, doi:10.1038/nphys758.

[42] Levina, A., Herrmann, J. M., and Geisel, T. Dynamical synapses causing self-organized criticality in neural networks. *Nat. Phys.*, **3** (2007), 857. Available from: http://dx.doi.org/10.1038/nphys758.

[43] Li, M. and Vitányi, P. *An introduction to Kolmogorov complexity and its applications*. Springer, New York (1993).

[44] Livi, R. On brain fluctuations and the challenges ahead. *Chaos Soliton Fract.*, **55** (2013), 60 . Available from: http://www.sciencedirect.com/science/article/pii/S0960077913000477.

[45] Lombardi, F., Herrmann, H. J., Perrone-Capano, C., Plenz, D., and de Arcangelis, L. Balance between excitation and inhibition controls the temporal organization of neuronal avalanches. *Phys. Rev. Lett.*, **108** (2012), 228703. Available from: http://link.aps.org/doi/10.1103/PhysRevLett.108.228703.

[46] London, M., Roth, A., Beeren, L., Hausser, M., and Latham, P. E. Sensitivity to perturbations in vivo implies high noise and suggests rate coding

in cortex. *Nature*, **466** (2010), 123. Available from: http://www.nature.com/nature/journal/v466/n7302/full/nature09086.html.

[47] Malmivuo, J. and Plonsey, R. *Bioelectromagnetism*. Oxford University Press, New York (1995).

[48] Massobrio, P., de Arcangelis, L., Pasquale, V., Jensen, H. J., and Plenz, D. Criticality as a signature of healthy neural systems. *Front. Syst. Neurosci.*, **9** (2015), 22. Available from: http://www.frontiersin.org/systems_neuroscience/10.3389/fnsys.2015.00022/full.

[49] Mejias, J. F., Kappen, H. J., and Torres, J. J. Irregular dynamics in up and down cortical states. *PLoS ONE*, **5** (2010), e13651. Available from: http://journals.plos.org/plosone/article?id=10.1371%2Fjournal.pone.0013651.

[50] Millman, D., Mihalas, S., Kirkwood, A., and Niebur, E. Self-organized criticality occurs in non-conservative neuronal networks during /'up/' states. *Nat. Phys.*, **6** (2010), 801. Available from: http://dx.doi.org/10.1038/nphys1757, doi:10.1038/nphys1757.

[51] Montbrió, E., Pazó, D., and Roxin, A. Macroscopic description for networks of spiking neurons. *Phys. Rev. X*, **5** (2015), 021028. Available from: http://link.aps.org/doi/10.1103/PhysRevX.5.021028.

[52] Monteforte, M. and Wolf, F. Dynamic flux tubes form reservoirs of stability in neuronal circuits. *Phys. Rev. X*, **2** (2012), 041007. Available from: http://link.aps.org/doi/10.1103/PhysRevX.2.041007.

[53] Olmi, S., Livi, R., Politi, A., and Torcini, A. Collective oscillations in disordered neural networks. *Phys. Rev. E*, **81** (2010), 046119. Available from: http://journals.aps.org/pre/abstract/10.1103/PhysRevE.81.046119.

[54] Ostojic, S. Two types of asynchronous activity in networks of excitatory and inhibitory spiking neurons. *Nat. Neurosci.*, **17** (2014), 594. Available from: http://www.nature.com/neuro/journal/v17/n4/full/nn.3658.html.

[55] Panzeri, S., Petersen, R. S., Schultz, S. R., Lebedev, M., and Diamond, M. E. The role of spike timing in the coding of stimulus location in rat somatosensory cortex. *Neuron*, **29** (2001), 769. Available from: http://www.sciencedirect.com/science/article/pii/S0896627301002513.

[56] Pazó, D. and Montbrió, E. From quasiperiodic partial synchronization to collective chaos in populations of inhibitory neurons with delay. *Phys. Rev. Lett.*, **116** (2016), 238101. Available from: http://link.aps.org/doi/10.1103/PhysRevLett.116.238101.

[57] Petermann, T., Thiagarajan, T. C., Lebedev, M. A., Nicolelis, M. A., Chialvo, D. R., and Plenz, D. Spontaneous cortical activity in awake monkeys composed of neuronal avalanches. *Proc. Natl. Acad. Sci. U.S.A.*, **106** (2009), 15921. Available from: http://www.pnas.org/content/106/37/15921.full.

[58] Petrosian, A. Kolmogorov complexity of finite sequences and recognition of different preictal eeg patterns. In *Proceedings of the Eighth IEEE Symposium on Computer-Based Medical Systems, Lubbock, Texas, 1995*, p. 212 (1995).

[59] Sanchez-Vives, M. V. and McCormick, D. A. Cellular and network mechanisms of rhythmic recurrent activity in neocortex. *Nat. Neurosci.*, **3** (2000), 1027. Available from: http://www.nature.com/neuro/journal/v3/n10/full/nn1000_1027.html.

[60] Segev, R., Shapira, Y., Benveniste, M., and Ben-Jacob, E. Observations and modeling of synchronized bursting in two-dimensional neural networks. *Phys. Rev. E*, **64** (2001), 011920. Available from: http://link.aps.org/doi/10.1103/PhysRevE.64.011920.

[61] Shimada, I. and Nagashima, T. A numerical approach to ergodic problem of dissipative dynamical systems. *Prog. Theor. Phys.*, **61** (1979), 1605. Available from: http://ptp.oxfordjournals.org/content/61/6/1605.abstract.

[62] Shu, Y., Hasenstaub, A., and McCormick, D. A. Turning on and off recurrent balanced cortical activity. *Nature*, **423** (2003), 288. Available from: http://www.nature.com/nature/journal/v423/n6937/full/nature01616.html.

[63] Touboul, J. and Destexhe, A.

[64] Touboul, J. and Destexhe, A. Can power-law scaling and neuronal avalanches arise from stochastic dynamics? *PLoS ONE*, **5** (2010), e8982. Available from: http://dx.doi.org/10.1371%2Fjournal.pone.0008982.

[65] Tsodyks, M. and Markram, H. The neural code between neocortical pyramidal neurons depends on neurotransmitter release probability. *Proc. Natl. Acad. Sci. U.S.A.*, **94** (1997), 719. Available from: http://www.pnas.org/content/94/2/719.abstract.

[66] Tsodyks, M., Pawelzik, K., and Markram, H. Neural networks with dynamic synapses. *Neural Comput.*, **10** (1998), 821. Available from: http://dx.doi.org/10.1162/089976698300017502.

[67] Tsodyks, M., Uziel, A., and Markram, H. Synchrony generation in recurrent networks with frequency-dependent synapses. *J. Neurosci.*, **20** (2000), 825. Available from: http://www.jneurosci.org/content/20/1/RC50.short.

[68] Ullner, E. and Politi, A. Self-sustained irregular activity in an ensemble of neural oscillators. *Phys. Rev. X*, **6** (2016), 011015. Available from: http://link.aps.org/doi/10.1103/PhysRevX.6.011015.

[69] van Vreeswijk, C. Partial synchronization in populations of pulse-coupled oscillators. *Phys. Rev. E*, **54** (1996), 5522. Available from: http://link.aps.org/doi/10.1103/PhysRevE.54.5522.

[70] van Vreeswijk, C. and Sompolinsky, H. Chaos in neuronal networks with balanced excitatory and inhibitory activity. *Science*, **274** (1996), 1724. Available from: http://science.sciencemag.org/content/274/5293/1724.

[71] Vogels, T. P., Rajan, K., and Abbott, L. Neural network dynamics. *Annu. Rev. Neurosci.*, **28** (2005), 357. Available from: http://dx.doi.org/10.1146/annurev.neuro.28.061604.135637.

[72] Volman, V., Baruchi, I., Persi, E., and Ben-Jacob, E. Generative modelling of regulated dynamical behavior in cultured neuronal networks. *Physica A*, **335** (2004), 249. Available from: http://www.sciencedirect.com/science/article/pii/S0378437103011154.

[73] Wang, X.-J. Neurophysiological and computational principles of cortical rhythms in cognition. *Physiol. Rev.*, **90** (2010), 1195. Available from: http://physrev.physiology.org/content/90/3/1195.long.

[74] Zillmer, R., Brunel, N., and Hansel, D. Very long transients, irregular firing, and chaotic dynamics in networks of randomly connected inhibitory integrate-and-fire neurons. *Phys. Rev. E*, **79** (2009), 031909. Available from: http://link.aps.org/doi/10.1103/PhysRevE.79.031909.

[75] Zillmer, R., Livi, R., Politi, A., and Torcini, A. Desynchronization in diluted neural networks. *Phys. Rev. E*, **74** (2006), 036203. Available from: http://link.aps.org/doi/10.1103/PhysRevE.74.036203.